current drug therapies used to treat occlusive respiratory disorders.

Authorship Contributions

Participated in research design: Ohba, Sawada, Imaizumi.

Conducted experiments: Ohba, Sawada, Suzuki.

Performed data analysis: Ohba, Sawada, Yamamura, Ohya, Imaizumi.

Wrote or contributed to the writing of the manuscript: Tsuda, Imaizumi.

References

Braiman A, Gold'Shtein V, and Priel Z (2000) Feasibility of a sustained steep Ca^{2+} Gradient in the cytosol of electrically non-excitable cells. *J Theor Biol* **206**:115–130.

Braiman A and Priel Z (2001) Intracellular stores maintain stable cytosolic Ca^{2+} gradients in epithelial cells by active Ca^{2+} redistribution. *Cell Calcium* **30**:361–371.

Braiman A and Priel Z (2008) Efficient mucociliary transport relies on efficient regulation of ciliary beating. *Respir Physiol Neurobiol* **163**:202–207.

Chang LY, Wu R, and Nettesheim P (1985) Morphological changes in rat tracheal cells during the adaptive and early growth phase in primary cell culture. *J Cell Sci* **74**:283–301.

Clark R and Proks P (2010) ATP-sensitive potassium channels in health and disease. *Adv Exp Med Biol* **654**:165–192.

Dymek EE and Smith EF (2007) A conserved CaM- and radial spoke associated complex mediates regulation of flagellar dynein activity. *J Cell Biol* **179**:515–526.

Evans JH and Sanderson MJ (1999) Intracellular calcium oscillations regulate ciliary beat frequency of airway epithelial cells. *Cell Calcium* **26**:103–110.

Flagg TP, Enkvetchakul D, Koster JC, and Nichols CG (2010) Muscle K_{ATP} channels: recent insights to energy sensing and myoprotection. *Physiol Rev* **90**:799–829.

Fukuse T, Hirata T, Omasa M, and Wada H (2002) Effect of adenosine triphosphate-sensitive potassium channel openers on lung preservation. *Am J Respir Crit Care Med* **165**:1511–1515.

Funabashi K, Ohya S, Yamamura H, Hatano N, Muraki K, Giles W, and Imaizumi Y (2010) Accelerated Ca^{2+} entry by membrane hyperpolarization due to Ca^{2+}-activated K^+ channel activation in response to histamine in chondrocytes. *Am J Physiol Cell Physiol* **298**:C786–C797.

Garlid KD, Paucek P, Yarov-Yarovoy V, Sun X, and Schindler PA (1996) The mitochondrial K_{ATP} channel as a receptor for potassium channel openers. *J Biol Chem* **271**:8796–8799.

Grimmsmann T and Rustenbeck I (1998) Direct effects of diazoxide on mitochondria in pancreatic β-cells and on isolated liver mitochondria. *Br J Pharmacol* **123**: 781–788.

Hibino H, Inanobe A, Furutani K, Murakami S, Findlay I, and Kurachi Y (2010) Inwardly rectifying potassium channels: their structure, function, and physiological roles. *Physiol Rev* **90**:291–366.

Holmuhamedov EL, Wang L, and Terzic A (1999) ATP-sensitive K^+ channel openers prevent Ca^{2+} overload in rat cardiac mitochondria. *J Physiol* **519**:347–360.

Imaizumi Y, Muraki K, and Watanabe M (1989) Ionic currents in single smooth muscle cells from the ureter of the guinea-pig. *J Physiol* **411**:131–159.

Kawakami M, Nagira T, Hayashi T, Shimamoto C, Kubota T, Mori H, Yoshida H, and Nakahari T (2004) Hypo-osmotic potentiation of acetylcholine-stimulated ciliary beat frequency through ATP release in rat tracheal ciliary cells. *Exp Physiol* **89**:739–751.

Leroy C, Dagenais A, Berthiaume Y, and Brochiero E (2004) Molecular identity and function in transepithelial transport of K_{ATP} channels in alveolar epithelial cells. *Am J Physiol Lung Cell Mol Physiol* **286**:L1027–L1037.

Lorenzo IM, Liedtke W, Sanderson MJ, and Valverde MA (2008) TRPV4 channel participates in receptor-operated calcium entry and ciliary beat frequency regulation in mouse airway epithelial cells. *Proc Natl Acad Sci USA* **105**:12611–12616.

Ma W, Silberberg SD, and Priel Z (2002) Distinct axonemal processes underlie spontaneous and stimulated airway ciliary activity. *J Gen Physiol* **120**:875–885.

Malerba M, Radaeli A, Mancuso S, and Polosa R (2010) The potential therapeutic role of potassium channel modulators in asthma and chronic obstructive pulmonary disease. *J Biol Regul Homeost Agents* **24**:123–130.

Morimoto T, Sakamoto K, Sade H, Ohya S, Muraki K, and Imaizumi Y (2007) Voltage-sensitive oxonol dyes are novel large-conductance Ca^{2+}-activated K^+ channel activators selective for β1 and β4 but not for β2 subunits. *Mol Pharmacol* **71**:1075–1088.

O'Grady SM and Lee SY (2003) Chloride and potassium channel function in alveolar epithelial cells. *Am J Physiol Lung Cell Mol Physiol* **284**:L689–L700.

O'Rourke B (2004) Evidence for mitochondrial K^+ channels and their role in cardioprotection. *Circ Res* **94**:420–432.

Pelaia G, Gallelli L, Vatrella A, Grembiale RD, Maselli R, De Sarro GB, and Marsico SA (2002) Potential role of potassium channel openers in the treatment of asthma and chronic obstructive pulmonary disease. *Life Sci* **70**:977–990.

Rodrigo GC and Standen NB (2005) ATP-sensitive potassium channels. *Curr Pharm Des* **11**:1915–1940.

Sakato M, Sakakibara H, and King SM (2007) Chlamydomonas outer arm dynein alters conformation in response to Ca^{2+}. *Mol Biol Cell* **18**:3620–3634.

Salathe M (2007) Regulation of mammalian ciliary beating. *Annu Rev Physiol* **69**: 401–422.

Salathe M and Bookman RJ (1999) Mode of Ca^{2+} action on ciliary beat frequency in single ovine airway epithelial cells. *J Physiol* **520**:851–865.

Schmid A and Salathe M (2011) Ciliary beat co-ordination by calcium. *Biol Cell* **103**: 159–169.

Seybold ZV, Mariassy AT, Stroh D, Kim CS, Gazeroglu H, and Wanner A (1990) Mucociliary interaction in vitro: effects of physiological and inflammatory stimuli. *J Appl Physiol* **68**:1421–1426.

Shiima-Kinoshita C, Min KY, Hanafusa T, Mori H, and Nakahari T (2004) β2-adrenergic regulation of ciliary beat frequency in rat bronchiolar epithelium: potentiation by isosmotic cell shrinkage. *J Physiol* **554**:403–416.

Tarasiuk A, Bar-Shimon M, Gheber L, Korngreen A, Grossman Y, and Priel Z (1995) Extracellular ATP induces hyperpolarization and motility stimulation of ciliary cells. *Biophys J* **68**:1163–1169.

Trinh NT, Privé A, Kheir L, Bourret JC, Hijazi T, Amraei MG, Noël J, and Brochiero E (2007) Involvement of K_{ATP} and KvLQT1 K^+ channels in EGF-stimulated alveolar epithelial cell repair processes. *Am J Physiol Lung Cell Mol Physiol* **293**:L870–L882.

Trinh NT, Privé A, Maillé E, Noël J, and Brochiero E (2008) EGF and K^+ channel activity control normal and cystic fibrosis bronchial epithelia repair. *Am J Physiol Lung Cell Mol Physiol* **295**:L866–L880.

Weiss T, Gheber L, Shoshan-Barmatz V, and Priel Z (1992) Possible mechanism of ciliary stimulation by extracellular ATP: involvement of calcium-dependent potassium channels and exogenous Ca^{2+}. *J Membr Biol* **127**:185–193.

Woo SK, Kwon MS, Ivanov A, Gerzanich V, and Simard JM (2013) The sulfonylurea receptor 1 (Sur1)-transient receptor potential melastatin 4 (Trpm4) channel. *J Biol Chem* **288**:3655–3667.

Yamada A, Gaja N, Ohya S, Muraki K, Narita H, Ohwada T, and Imaizumi Y (2001) Usefulness and limitation of $DiBAC_4(3)$, a voltage-sensitive fluorescent dye, for the measurement of membrane potentials regulated by recombinant large conductance Ca^{2+}-activated K^+ channels in HEK293 cells. *Jpn J Pharmacol* **86**:342–350.

Yamada M and Kurachi Y (2005) A functional role of the C-terminal 42 amino acids of SUR2A and SUR2B in the physiology and pharmacology of cardiovascular ATP-sensitive K^+ channels. *J Mol Cell Cardiol* **39**:1–6.

Yamamura H, Ikeda C, Suzuki Y, Ohya S, and Imaizumi Y (2012) Molecular assembly and dynamics of fluorescent protein-tagged single $K_{Ca}1.1$ channel in expression system and vascular smooth muscle cells. *Am J Physiol Cell Physiol* **302**: C1257–C1268.

Yamazaki D, Kito H, Yamamoto S, Ohya S, Yamamura H, Asai K, and Imaizumi Y (2011) Contribution of $K_{ir}2$ potassium channels to ATP-induced cell death in brain capillary endothelial cells and reconstructed HEK293 cell model. *Am J Physiol Cell Physiol* **300**:C75–C86.

Address correspondence to: Dr. Yuji Imaizumi, Department of Molecular and Cellular Pharmacology, Graduate School of Pharmaceutical Sciences, Nagoya City University, 3-1 Tanabedori, Mizuhoku, Nagoya 467-8603, Japan. E-mail: yimaizum@phar.nagoya-cu.ac.jp

The Journal of Toxicological Sciences (J. Toxicol. Sci.)
Vol.39, No.3, ***-***, 2014

Original Article

MWCNT causes extensive damage to the ciliated epithelium of the trachea of rodents

Teruya Ohba[1], Jiegou Xu[2], David B. Alexander[2], Akane Yamada[1], Jun Kanno[3], Akihiko Hirose[4], Hiroyuki Tsuda[2] and Yuji Imaizumi[1]

[1]Department of Molecular and Cellular Pharmacology, Nagoya City University Graduate School of Pharmaceutical Sciences, 3-1 Tanabedori, Mizuhoku, Nagoya 467-8603, Japan
[2]Laboratory of Nanotoxicology, Nagoya City University, 3-1 Tanabedori, Mizuhoku, Nagoya 467-8603, Japan
[3]Division of Cellular and Molecular Toxicology, 1-18-1 Kamiyoga, Setagaya-ku, Tokyo 158-8501, Japan
[4]Division of Risk Assessment, National Institute of Health Sciences, 1-18-1 Kamiyoga, Setagaya-ku, Tokyo 158-8501, Japan

(Received February 19, 2014; Accepted April 8, 2014)

ABSTRACT — The ciliated tracheobronchial epithelium plays an important role in the excretion of inhaled dust. While many reports indicate that inhaled multi-walled carbon nanotubes (MWCNT) induce inflammation and proliferative changes in the lung and pleura, their effects on the upper airway have not been reported. Two different types of MWCNTs, MWCNT-L (8 μm in length and 150 nm in diameter) and MWCNT-S (3 μm in length and 15 nm in diameter), were examined for their effect on the trachea as well as the bronchus and lung. *In vitro*, the movement of the cilia of primary tracheal epithelial cells was impaired by treatment with the 2 MWCNTs. Rats were treated with 0.3 ml of a 250 μg/ml suspension of MWCNTs on days 1, 4, and 7, and sacrificed on day 8. Extensive loss of ciliated cells and replacement by flat cells without cilia was observed in the trachea. Deposition of MWCNTs and occasional squamous cell metaplasia were found in the regenerative granulation tissue. The proportion of the lesion to the transverse section of the trachea was vehicle, 0; MWCNT-L, 27.2 ± 10.5; MWCNT-S, 32.1 ± 15.8 (both MWCNTs, $p < 0.001$ vs vehicle). The amount of cilia showed significant decrease in the MWCNT-L treated rats ($p < 0.05$). In contrast to the trachea lesions, the number of inflammatory foci in the lung was greater in the MWCNT-S than in the MWCNT-L treated rats. Our results indicate that both MWCNTs caused extensive damage to the ciliated epithelium of the trachea. This damage may prolong the deposition of inhaled MWNCT in the lung.

Key words: MWCNT, Tracheal damage, Ciliated epithelium, Rat

INTRODUCTION

Multi-walled carbon nanotubes (MWCNT) are a newly developed material with potential applications in many fields including the biomedical field. The high aspect ratio of MWCNT is similar to that of asbestos and has led to concern that exposure to MWCNT might cause asbestos-like lung diseases (Bonner, 2010; Donaldson *et al.*, 2010; Nagai and Toyokuni, 2010). Many reports have indicated that exposure of rats to MWCNT induces inflammation, fibrosis and oxidative stress in the lung and pleura (Mercer *et al.*, 2010, 2013; Xu *et al.*, 2012). To date, *in vivo* studies have focused on the toxicity of MWCNT in the lung and pleura, and nothing has been reported regarding the effect of MWCNT on the epithelium of the trachea.

The tracheal and primary branch of the bronchial epithelium is mainly composed of ciliated cells and some goblet cells. The ciliated cells are responsible for carrying out inhaled dust particles in the throat by their ciliary transportation movement. Thus, the ciliated cells play a pivotal role in the defense of the airway against inhaled particle matter. Several environmental factors such as cigarette smoke (Simet *et al.*, 2010) and diesel gas particles (Li *et al.*, 2011) have been shown to impair ciliated cell functions, resulting in increased pulmonary deposition. Zinc oxide nanoparticles have been reported to induce proliferation of airway epithelial cells and goblet cell hyperplasia (Cho *et al.*, 2011) and transient epithelial hyperplasia of the terminal bronchiole (Xu *et al.*,

Correspondence: Yuji Imaizumi (E-mail: yimaizum@phar.nagoya-cu.ac.jp)

2013). Although several reports indicate that MWCNT have some toxic effects on bronchial epithelial cells *in vitro* (Hirano *et al.*, 2010; Lindberg *et al.*, 2009; Rotoli *et al.*, 2008), the effect on the upper airway in animals remains unknown. In the present study, we investigated the effects of MWCNT on the tracheal epithelium *in vitro* and *in vivo* and the bronchus and lung *in vivo* after short-term exposure.

MATERIALS AND METHODS

Animals

8-12 week old C57BL/6N male mice (Japan SLC Inc., Shizuoka, Japan) and 6-7 week old Wistar/ST rats were obtained from Japan SLC Inc. Rats were housed in the Animal Center of Nagoya City University Graduate School of Pharmaceutical Sciences and maintained on a 12 hr light/12 hr dark cycle and received Oriental MF basal diet (Oriental Yeast Co. Ltd., Tokyo, Japan) and water *ad libitum*. The study was conducted according to the Guidelines for the Care and Use of Laboratory Animals of Nagoya City University Graduate School of Pharmaceutical Sciences, and the experimental protocol was approved by the Nagoya City University Animal Care and Use Committee (H24-p-12).

Preparation of MWCNT and Fluorescent Microspheres (FMS)

We used two types of MWCNTs, MWCNT-L and MWCNT-S, which are grown in the vapor phase. According to the manufacturer's information, the primary size of MWCNT-L is 150 nm in mean diameter and 8 μm in mean length, and the primary size of MWCNT-S is 15 nm in mean diameter and 3 μm in mean length. Five milligrams of MWCNT-L or MWCNT-S were suspended in 20 ml of saline containing 0.5% Pluronic F68 (PF68, non-ionic, biocompatible amphiphillic block copolymers, Sigma-Aldrich, St Louis, MO, USA) and homogenized for 1 min at 3,000 rpm in a Polytron PT1600E benchtop homogenizer (Kinematika AG, Littau, Switzerland) 4 times. The suspensions were sonicated for 30 min shortly before use to minimize aggregation. The concentration of the MWCNTs was 250 μg/ml. Both MWCNT-L and MWCNT-S dispersed well in the vehicle solution. MWCNT-L showed single fibers with a needle-like shape under scanning electron microscope (SEM) observation, but gradually formed agglomerates over time. Since MWCNT-S are tangled fibers, it showed cotton-like aggregation in suspension under SEM observation. However, they did not form larger agglomerates: incubation in suspension up to 7 days (data not shown). Fluorescent Microspheres (FMS) were purchased from Invitrogen (TetraSpeckTM microspheres, 500 nm in diameter) and suspended by sonication at 250 μg/ml in saline containing 0.5% PF68.

Isolation of single ciliated cells

Isolation of single ciliated cells was as previously reported (Ma *et al.*, 2006). Briefly, the tracheal epithelium was separated from the cartilage and cut into pieces of approximately 0.1 × 0.1 cm. The tissue was incubated in phosphate-buffered saline containing NaCl 137 mM, KCl 2.7 mM, $CaCl_2$ 0.9 mM, $MgCl_2$ 0.5 mM, Na_2HPO_4 8 mM, KH_2PO_4 1.47 mM and d-glucose 5 mM, pH 7.4 (PBS-g) supplemented with 13 U/ml papain (Sigma), 1 mg/ml bovine serum albumin (Sigma-Aldrich) and 1 mg/ml 1,4-dithiothreitol (Wako Chemicals Co. Ltd., Osaka, Japan). Cells were then dispersed several times with a fire-polished Pasteur pipette and re-suspended in PBS-g and used immediately.

In vitro study

The isolated mouse tracheal epithelial cells were maintained in high glucose Dulbecco's modified Eagle's medium (DMEM, Sigma) supplemented with 10% fetal bovine serum (FBS), 1 U/ml penicillin G, and 0.1 mg/ml streptomycin sulfate, at 37°C, 5% CO_2. The cells were then exposed for 10 min to vehicle, FMS, MWCNT-L, or MWCNT-S in FMS or MWCNT suspensions to a final concentration of 10 μg/ml. Media was then replaced by fresh media. The cells were observed 10 min and 12 and 18 hr after addition of fresh media and the proportion of cells with ciliary movement per total ciliated cells was determined. For each group, approximately 500 cells per dish in three separate dishes were counted.

Rat study

Male Wistar rats aged 6-7 weeks were treated with 0.3 ml of 250 μg/ml MWCNT-L or MWCNT-S (3 rats each) suspended in PF68 vehicle on days 1, 4, and 7. The suspension was administered by a microsprayer (series IA-1B Intratracheal Aerosolizer; Penn-century, Philadelphia, PA, USA) with the tip of the microsprayer just inside the entrance of the trachea (Xu *et al.*, 2012). Administration was done in synchronization with spontaneous inhalation. The rats were sacrificed 24 hr after the last dosing (day 8) under deep anesthesia with isoflurane. The trachea, bronchus and lung were excised and fixed in 4% paraformaldehyde solution. The trachea was transversely cut into 3 pieces, upper, middle and lower parts, and the tracheal sections and the bronchus and lungs were routinely processed for paraffin embedding, sectioning and histological examination.

Histology and Immunostaining

Haematoxylin-Eosin (H&E) stained slides of the trachea; bronchus and lung were examined by board pathologists. The epithelial lesions in each tracheal section were measured with the image analyzing function (Nikon, Tokyo, Japan) and expressed as the ratio of the length of the lesion to the whole length of the tracheal section. The number of granulation foci of the lung sections were counted and expressed as number/cm^2 lung tissue. Localization of MWCNT fibers in the trachea and lung tissue were determined with polarized light microscopy (Olympus BX51N-31P-O, Tokyo, Japan) at × 400 and × 1,000 magnification. Immunostaining of acetyled tublin, a specific marker for cilia, was performed using mouse polyclonal anti-acetyled tublin antibody (Sigma Aldrich). The antibody was diluted 1:1,000 in PBS containing 5% goat albumin and applied to deparaffinized and blocked slides, and the slides were incubated at 4°C overnight. The next day, the slides were washed 3 times in PBS and then incubated for 2 hr with Alexa 488-conjugated goat anti-mouse IgG (Molecular Probe, Eugene, USA) diluted 1:1,000. After washing 3 times in PBS, the slides were counterstained with DAPI (Vector laboratories, USA). Immunostained sections were observed using an A1R laser scanning confocal microscope (Nikon). The ratio of the fluorescent intensity of acetyled tublin in the top layer of cells of the tracheal ciliated epithelium to the fluorescent intensity of DAPI in the underlying submucosal tissue was measured. This ratio was used to compare the intensity of acetyled tublin fluorescence in the different samples. Fluorescence intensity was determined with NIS Elements software (version 3.10; Nikon).

Statistical Analysis

Statistical significance was examined using Tukey's test. *P* values less than 0.05 were considered to be statistically significant.

RESULTS

In vitro study

Cultures of ciliated cells were incubated in growth media with vehicle (PF68), fluorescent microspheres (FMS), or MWCNT for 10 min. During the 10 min incubation in media containing FMS, FMS in contact with the cilia and/or cell surface could readily be located (white arrow in Fig. 1A in bottom panel), however, 10 min after replacing the FMS containing media with standard growth media, cell-associated FMS could no longer be found. In contrast, ten min after replacing the MWCNT

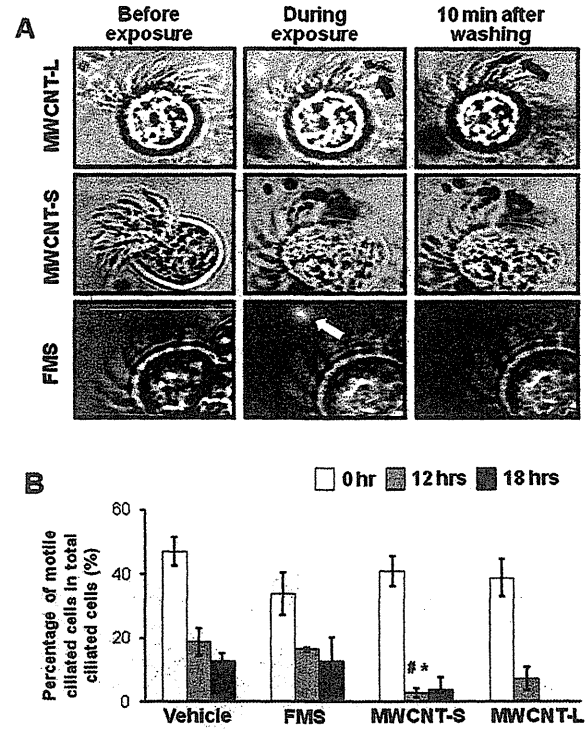

Fig. 1. Exposure of MWCNT to isolated tracheal ciliated cells *in vitro*. A, Images of ciliated cells exposed to fluorescent microsphere (FMS), MWCNT-L, and MWCNT-S; left, before exposure; middle, during exposure; right, after media change. FMS (white arrow) was clearly removed. MWCNTs were not removed (black arrows). Bars equal 5 μm. B, Percentage of cells with active cilia at time 0 and 12 and 18 hr after media change. n = 3; * $p < 0.05$ vs vehicle control, # $p < 0.05$ vs FMS control.

containing media with standard growth media, MWCNT-L and MWCNT-S fibers were not detached from the ciliated cells and could be observed associated with the cilia and/or cell surface (black arrows in Fig. 1A). In the cilia activity test, FMS did not reduce the percentage of cells with active cilia compared to the vehicle group (Fig. 1B). However, the percentage of cells with active cilia in the MWCNT-L treated group was significantly reduced (2.73 ± 1.37; n = 3, $p < 0.05$) compared to the vehicle (18.7 ± 4.28) and FMS (16.50 ± 0.67) groups after 12 hr. Although not significant, a similar decrease was also observed in the MWCNT-S group.

Rat study

The majority of the epithelium of the trachea is com-

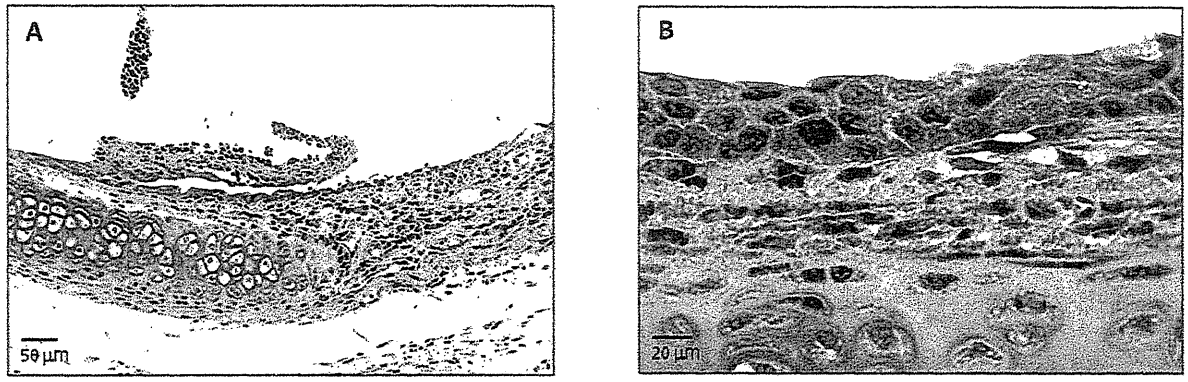

Fig. 2. Erosive lesions and squamous cell metaplasia. A, Representative image showing erosive lesions induced by treatment of MWCNT-L or MWCNT-S; B, Representative image of squamous cell metaplsia.

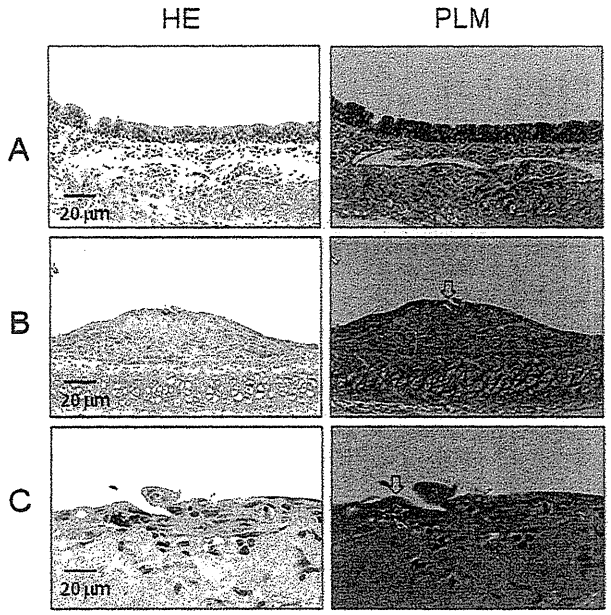

Fig. 3. Tracheal lesions in rat treated with MWCNT-L. A, Undamaged tracheal ciliated epithelium; B, An erosive lesion with granulation tissue underneath the thin regenerating epithelium; C, A higher magnification image of the lesion in B. MWCNT-L fibers (open arrows) can be clearly observed in the granulation tissue by polarized light microscopy (PLM).

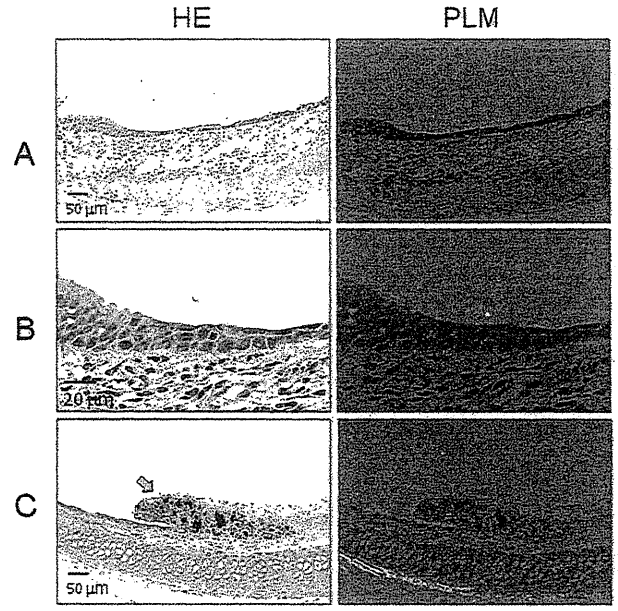

Fig. 4. Tracheal lesions in a rat treated with MWCNT-S. A, Tracheal epithelium showing a transition from undamaged ciliated epithelium to regenerating flat epithelium overlying edematous granulation tissue. B, A higher magnification image of the lesion in B. C, An erosive lesion with granulation tissue containing many black MWCNT-S fibers. MWCNT-S fibers are not visualized by polarized light microscopy (PLM).

posed of single layer of columnar ciliated cells. Treatment with MWCNT-L induced marked damage to the surface ciliated cells resulting in erosive changes (Fig. 2A) and replacement with flat cells without cilia and occasional squamous cell metaplasia (Fig. 2B). An increase in goblet cells was found in the columnar ciliated cell area, although goblet cell damage was not obvious. MWCNT-L fiber aggregates were frequently observed in the lesions (Figs. 3B and 3C) but not in the healthy mucosa (Fig. 3A). MWCNT-S caused similar mucosal damage (Fig. 4,

Table 1. Lesions in the tracheal epithelium and lung

Treatment	No. of rats	Tracheal epithelium			Lung
		Erosion	Regenerated cells		
		Incidence (%)	Incidence (%)	Proportion [a] (%)	Granulation tissue (No./cm²) [b]
Vehicle	4	0	0	0	0
MWCNT-L	3	100 ***	100 ***	27.2 ± 8.7**	0.1 ± 0.1
MWCNT-S	4	25 ***	100 ***	32.7 ± 11.5**	1.0 ± 0.2 **,##

Notes: [a], the length of the regenerated lesion in the whole length of the transverse tracheal circle; [b], the number of the granulation per square centimeter of the lung tissue; ** and *** represent p values < 0.01 and 0.001, vs the vehicle; ## represents p values < 0.01, vs MWCNT-L

left panel) but, because of lack of MWCNT-S mediated polarization, the fibers could not be detected by polarized light microscopy (Fig. 4C, right panel).

Table 1 shows the incidences of the erosion, incidences and the percentage of the length of the tracheal lesions compared to the total length of the tracheal cross section from rats administered vehicle or MWCNT. Tracheal lesions in rats administered MWCNT-L (27.2 ± 10.5) or MWCNT-S (32.1 ± 15.8) were significantly greater than in rats administered vehicle alone ($p < 0.001$ for both comparisons). No difference was found between the MWCNT-L and MWCNT-S groups. Although not significant, the value for MWCNT-L administered rats was greater than for MWCNT-S administered rats.

The ratio of fluorescence of acetyled tublin on the surface of the trachea (0.48 ± 0.06) to submucosal DAPI fluorescence significantly decreased ($p < 0.05$) in rats treated with MWCNT-L (Fig. 5). The value for the MWCNT-S treated rats showed a similar decrease but was not significant. The results clearly indicate the quantitative loss of ciliated cells by treatment with MWCNT-L.

In the lung, granulation foci composed of macrophages and fibrotic cells surrounding MWCNT aggregates was found (Fig. 6). Table 1 shows the number of granulation foci in the lungs of rats administered vehicle or MWCNT. The number of lesions in both the MWCNT-L and MWCNT-S administered groups were significantly higher than in the vehicle control group ($p < 0.001$ for both comparisons). The lesion count in the MWCNT-S group (1.04 ± 0.18) was significantly greater than the MWCNT-L group (0.06 ± 0.06) ($p < 0.05$) (Table 1).

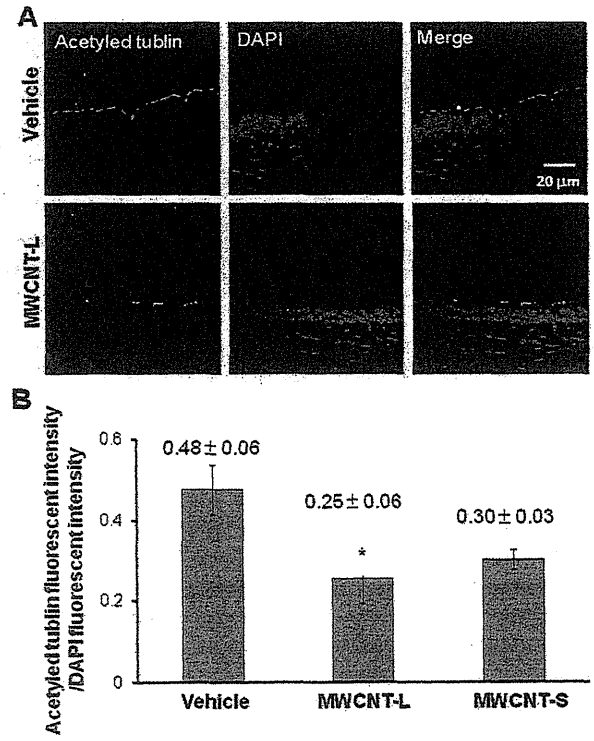

Fig. 5. Decrease in the proportion of ciliated cells in the bronchial epithelium. A, Representative images of immunostaining with anti-acetylated tubulin staining the cilia (left), DAPI (middle) and merged image (right); B, The ratio of the intensity of acetyled tublin to DAPI was decreased in the MWCNT-L group. n = 3~4; * $p < 0.05$ vs the vehicle.

DISCUSSION

The tracheobronchial ciliated epithelium is the first defense line against inhaled dust particles. The dust particles are transported from the lung alveoli through the bronchi and trachea toward the laryngopharynx by its directed ciliary movement. Pathologic changes in the bronchial epithelium such as goblet cell hyperplasia and

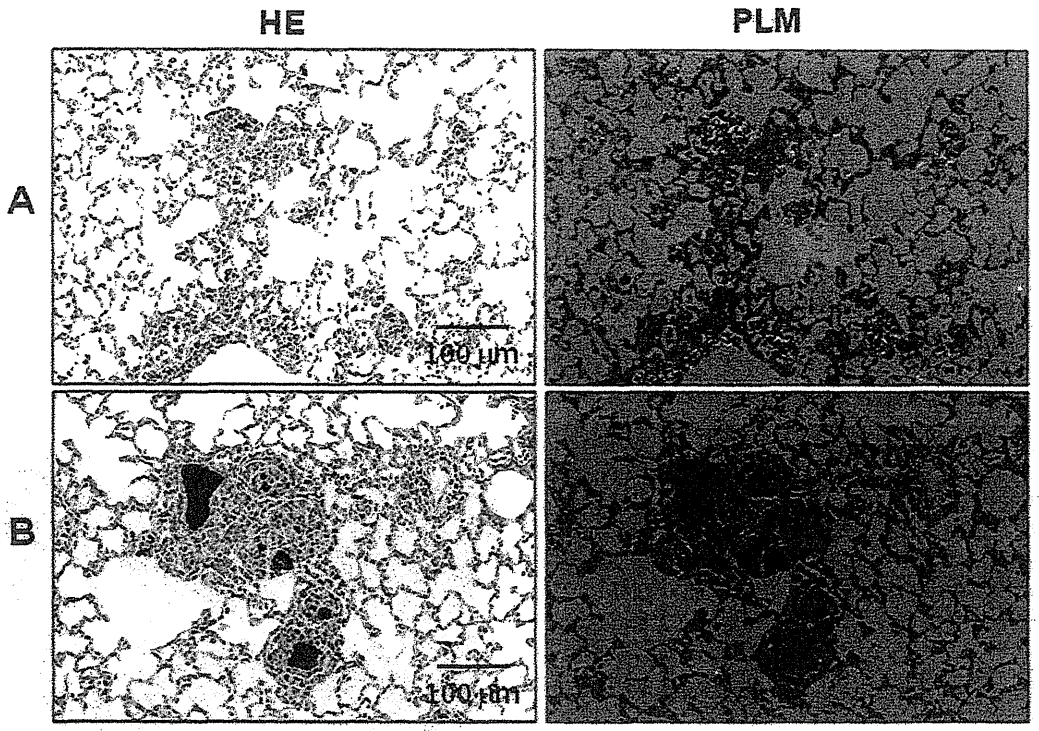

Fig. 6. Demonstration of MWCNTs in the lung tissue. HE and polarized images of the lung tissue treated with MWCNT-L (A) or MWCNT-S (B). Large aggregations of MWNNT-S (black mass) are found encapsulated in granulation tissue and small particles are found in alveolar macrophages. As in the trachea, MWCNT-S is not visualized by polarized light microscopy (PLM).

squamous cell metaplasia have been found by studies with particles such as ZnO particles (Choe *et al.*, 1997) and cigarette smoke (Neugut, 1988) and in some disease conditions such as bronchial asthma and chronic bronchitis (Aikawa *et al.*, 1992). The ciliated cell damage in these lesions causes impaired mucociliary protection and increases deposition of particles and microorganisms in the lung, causing inflammatory changes. These alterations may cause chronic injury and cell regeneration leading to an increase in carcinogenesis in the trachea, bronchi and lung.

This is the first report to show that MWCNTs cause extensive damage and loss of ciliated epithelium in the trachea followed by compensatory regeneration of cells without cilia including metaplastic squamous cells. *In vitro* observation clearly indicated that MWCNT caused impaired function of ciliated cells, potentially resulting in decreased clearance of the fibers from the lung, such as observed in studies of other fibers such as asbestos (Woodworth *et al.*, 1983). Decreased clearance of MWCNT would increase the retention time of the MWCNTs in the trachea and lung, which, in turn, would maintain the toxic effect, leading to even more loss of ciliated cells. This would increase the risk of spread of MWCNT to other organs, especially to the pleural cavity.

It should be noted that damage to the lung differed in MWCNT-L and MWCNT-S administered rats. Inflammatory changes, as evinced by an increase in granulation tissue in the lung, were more extensive in MWCNT-S administered rats. This indicates that there is an organotropic toxic effect of MWCNT. This may be related to their size and shape; however, further studies are necessary to elucidate the mechanism of this difference.

AKNOWLEDGMENTS

This study was supported by Grants-in-Aids by the Ministry of Health, Labour and Welfare, Japan: Risk of Chemical Substance 21340601 (H22-kagaku-ippan-005) and 2524301 (H25-kagaku-ippan-004).

REFERENCES

Aikawa, T., Shimura, S., Sasaki, H., Ebina, M. and Takishima, T. (1992): Marked goblet cell hyperplasia with mucus accumulation in the airways of patients who died of severe acute asthma attack. Chest, **101**, 916-921.

Bonner, J.C. (2010): Nanoparticles as a potential cause of pleural and interstitial lung disease. Proc. Am. Thorac. Soc., **7**, 138-141.

Cho, W.S., Duffin, R., Howie, S.E., Scotton, C.J., Wallace, W.A., Macnee, W., Bradley, M., Megson, I.L. and Donaldson, K. (2011): Progressive severe lung injury by zinc oxide nanoparticles; the role of Zn2+ dissolution inside lysosomes. Part Fibre. Toxicol., **8**, 27.

Choe, N., Tanaka, S., Xia, W., Hemenway, D.R., Roggli, V.L. and Kagan, E. (1997): Pleural macrophage recruitment and activation in asbestos-induced pleural injury. Environ. Health Perspect., **105 Suppl. 5**, 1257-1260.

Donaldson, K., Murphy, F.A., Duffin, R. and Poland, C.A. (2010): Asbestos, carbon nanotubes and the pleural mesothelium: a review of the hypothesis regarding the role of long fibre retention in the parietal pleura, inflammation and mesothelioma. Part. Fibre. Toxicol., **7**, 5.

Hirano, S., Fujitani, Y., Furuyama, A. and Kanno, S. (2010): Uptake and cytotoxic effects of multi-walled carbon nanotubes in human bronchial epithelial cells. Toxicol. Appl. Pharmacol., **249**, 8-15.

Li, J., Kanju, P., Patterson, M., Chew, W.L., Cho, S.H., Gilmour, I., Oliver, T., Yasuda, R., Ghio, A., Simon, S.A. and Liedtke, W. (2011): TRPV4-mediated calcium influx into human bronchial epithelia upon exposure to diesel exhaust particles. Environ. Health Perspect., **119**, 784-793.

Lindberg, H.K., Falck, G.C., Suhonen, S., Vippola, M., Vanhala, E., Catalan, J., Savolainen, K. and Norppa, H. (2009): Genotoxicity of nanomaterials: DNA damage and micronuclei induced by carbon nanotubes and graphite nanofibres in human bronchial epithelial cells *in vitro*. Toxicol. Lett., **186**, 166-173.

Ma, W., Korngreen, A., Weil, S., Cohen, E.B., Priel, A., Kuzin, L., and Silberberg, S.D. (2006): Pore properties and pharmacological features of the P2X receptor channel in airway ciliated cells. J. Physiol., **571**, 503-517.

Mercer, R.R., Hubbs, A.F., Scabilloni, J.F., Wang, L., Battelli, L.A., Schwegler-Berry, D., Castranova, V. and Porter, D.W. (2010): Distribution and persistence of pleural penetrations by multi-walled carbon nanotubes. Part. Fibre. Toxicol., **7**, 28.

Mercer, R.R., Scabilloni, J.F., Hubbs, A.F., Wang, L., Battelli, L.A., McKinney, W., Castranova, V. and Porter, D.W. (2013): Extrapulmonary transport of MWCNT following inhalation exposure. Part. Fibre. Toxicol., **10**, 38.

Nagai, H. and Toyokuni, S. (2010): Biopersistent fiber-induced inflammation and carcinogenesis: lessons learned from asbestos toward safety of fibrous nanomaterials. Arch. Biochem. Biophys., **502**, 1-7.

Neugut, A.I. (1988): Squamous cell cancers and cigarette smoke: a matter of exposure. Med. Hypotheses., **26**, 9-10.

Rotoli, B.M., Bussolati, O., Bianchi, M.G., Barilli, A., Balasubramanian, C., Bellucci, S. and Bergamaschi, E. (2008). Non-functionalized multi-walled carbon nanotubes alter the paracellular permeability of human airway epithelial cells. Toxicol. Lett., **178**, 95-102.

Simet, S.M., Sisson, J.H., Pavlik, J.A., Devasure, J.M., Boyer, C., Liu, X., Kawasaki, S., Sharp, J.G., Rennard, S.I. and Wyatt, T.A. (2010): Long-term cigarette smoke exposure in a mouse model of ciliated epithelial cell function. Am. J. Respir. Cell. Mol. Biol., **43**, 635-640.

Woodworth, C.D., Mossman, B.T. and Craighead, J.E. (1983): Squamous metaplasia of the respiratory tract. Possible pathogenic role in asbestos-associated bronchogenic carcinoma. Laboratory investigation; a journal of technical methods and pathology, **48**, 578-584.

Xu, J., Futakuchi, M., Alexander, D.B., Fukamachi, K., Numano, T., Suzui, M., Shimizu, H., Omori, T., Kanno, J., Hirose, A. and Tsuda, H. (2013): Nanosized zinc oxide particles do not promote DHPN-induced lung carcinogenesis but cause reversible epithelial hyperplasia of terminal bronchioles. Arch. Toxicol., **88**, 65-75.

Xu, J., Futakuchi, M., Shimizu, H., Alexander, D.B., Yanagihara, K., Fukamachi, K., Suzui, M., Kanno, J., Hirose, A., Ogata, A., Sakamoto, Y., Nakae, D., Omori, T. and Tsuda, H. (2012): Multi-walled carbon nanotubes translocate into the pleural cavity and induce visceral mesothelial proliferation in rats. Cancer Sci., **103**, 2045-2050.

RESEARCH ARTICLE

Comparative Study of Toxic Effects of Anatase and Rutile Type Nanosized Titanium Dioxide Particles *in vivo* and *in vitro*

Takamasa Numano[1,3], Jiegou Xu[2], Mitsuru Futakuchi[1], Katsumi Fukamachi[1], David B Alexander[2], Fumio Furukawa[3], Jun Kanno[4], Akihiko Hirose[4], Hiroyuki Tsuda[2], Masumi Suzui[1]*

Abstract

Two types of nanosized titanium dioxide, anatase ($anTiO_2$) and rutile ($rnTiO_2$), are widely used in industry, commercial products and biosystems. TiO_2 has been evaluated as a Group 2B carcinogen. Previous reports indicated that $anTiO_2$ is less toxic than $rnTiO_2$, however, under ultraviolet irradiation $anTiO_2$ is more toxic than $rnTiO_2$ *in vitro* because of differences in their crystal structures. In the present study, we compared the *in vivo* and *in vitro* toxic effects induced by $anTiO_2$ and $rnTiO_2$. Female SD rats were treated with 500 μg/ml of $anTiO_2$ or $rnTiO_2$ suspensions by intra-pulmonary spraying 8 times over a two week period. In the lung, treatment with $anTiO_2$ or $rnTiO_2$ increased alveolar macrophage numbers and levels of 8-hydroxydeoxyguanosine (8-OHdG); these increases tended to be lower in the $anTiO_2$ treated group compared to the $rnTiO_2$ treated group. Expression of MIP1α mRNA and protein in lung tissues treated with $anTiO_2$ and $rnTiO_2$ was also significantly up-regulated, with MIP1α mRNA and protein expression significantly lower in the $anTiO_2$ group than in the $rnTiO_2$ group. In cell culture of primary alveolar macrophages (PAM) treated with $anTiO_2$ and $rnTiO_2$, expression of MIP1α mRNA in the PAM and protein in the culture media was significantly higher than in control cultures. Similarly to the *in vivo* results, MIP1α mRNA and protein expression was significantly lower in the $anTiO_2$ treated cultures compared to the $rnTiO_2$ treated cultures. Furthermore, conditioned cell culture media from PAM cultures treated with $anTiO_2$ had less effect on A549 cell proliferation compared to conditioned media from cultures treated with $rnTiO_2$. However, no significant difference was found in the toxicological effects on cell viability of ultra violet irradiated $anTiO_2$ and $rnTiO_2$. In conclusion, our results indicate that $anTiO_2$ is less potent in induction of alveolar macrophage infiltration, 8-OHdG and MIP1α expression in the lung, and growth stimulation of A549 cells *in vitro* than $rnTiO_2$.

Keywords: Nanosized titanium dioxide - anatase - rutile - lung toxicity - MIP1α

Asian Pac J Cancer Prev, **15 (2)**, 929-935

Introduction

There are three mineral forms of natural titanium dioxide particles: rutile, anatase and brookite. Engineered anatase and rutile nanosized titanium dioxide particles ($anTiO_2$ and $rnTiO_2$) are being manufactured in large quantities worldwide and applied in many fields including material industry, electronic industry, commercial products and biosystems. Due to differences in crystal structure, $anTiO_2$ has better photocatalytic activity than $rnTiO_2$ (Kakinoki et al., 2004). Accordingly, $anTiO_2$ is mainly used in paints, such as surface painting of the walls and windows of buildings and vehicles, and photocatalytic systems, while $rnTiO_2$ is preferentially used in cosmetics, sunscreen and food additives.

Large quantity production and widespread application of $nTiO_2$ have given rise to concern about its health and environmental effects. Anatase and rutile type titanium dioxide particles, nanosized and larger, are evaluated as Group 2B carcinogens (possibly carcinogenic to humans) by WHO/International Agency for Research on Cancer (IARC, 2010), based on 2-year animal aerosol inhalation studies (Mohr et al., 2006). Pulmonary exposure to $rnTiO_2$ promotes DHPN-induced lung carcinogenesis in rats, and the promotion effect is possibly associated with $rnTiO_2$ burdened alveolar macrophage derived macrophage inflammatory protein 1 alpha (MIP1α), which acts as a growth factor to stimulate the proliferation of human lung adenocarcinoma cells (A549) *in vitro* (Xu et al., 2010). Dermal application of $anTiO_2$ has been shown to cause significant increases in the level of superoxide dismutase and malondialdehyde in hairless mice (Wu et al., 2009).

Size and photoactivation affect the *in vitro* toxicity of $anTiO_2$ and $rnTiO_2$. $anTiO_2$ (10 and 20 nm) induces

[1]*Department of Molecular Toxicology, Nagoya City University Graduate School of Medical Sciences and Medical School,* [2]*Laboratory of Nanotoxicology Project, Nagoya City University, Nagoya,* [3]*DIMS Institute of Medical Science, Aichi,* [4]*National Institute of Health Sciences, Tokyo, Japan* **For correspondence: suzui@med.nagoya-cu.ac.jp*

oxidative DNA damage, lipid peroxidation and micronuclei formation, and increases hydrogen peroxide and nitric oxide production in BEAS-2B cells, a human bronchial epithelial cell line, but anTiO$_2$ 200 nm particles do not (Gurr et al., 2005). In contrast, both nano-sized and 200nm ruTiO$_2$ are toxic *in vitro* (Gurr et al., 2005; Sayes et al., 2006). On the other hand, under ultraviolet irradiation, anTiO$_2$ is 100 times more toxic to human dermal fibroblasts and A549 cells than rnTiO$_2$, and is more potent than rnTiO$_2$ in the induction of lactate dehydrogenase release, reactive oxygen species production and interleukin 8 secretion (Sayes et al., 2006). Experimental data demonstrating differences in the toxic effects of anTiO$_2$ and rnTiO$_2$ *in vivo*, however, are still lacking.

Respiratory exposure to nTiO$_2$ particles can occur both at the workplace, e.g., in manufacturing and packing sites, and outside the workplace during their use (Maynard et al., 2006; Schulte et al., 2008). In the present study, we delivered anTiO$_2$ and rnTiO$_2$ to the rat lung by trans-tracheal intra-pulmonary spraying (TIPS) and compared lung inflammation and several toxicological parameters induced by anTiO$_2$ and rnTiO$_2$. The results indicated that obvious lung inflammatory lesions were not observed in the rats, and anTiO$_2$ or rnTiO$_2$ particles were phagocytosed by alveolar macrophages. Analysis of alveolar macrophage induction, 8-OHdG level in the lung, and MIP1α expression both *in vivo* in the lung and *in vitro* in PAM indicated that anTiO$_2$ elicited lower levels of biological responses than rnTiO$_2$. Long-term toxic effects of anTiO$_2$ and rnTiO$_2$ still need to be clarified.

Materials and Methods

Preparation and characterization of nTiO$_2$ suspension

Nanosized TiO$_2$ particles (anatase type without coating, primary size 25 nm and rutile type without coating, primary size 20 nm) were provided by Japan Cosmetic Association, Tokyo, Japan. Both anTiO$_2$ and rnTiO$_2$ particles were suspended in saline at 500 μg/ml and then autoclaved. The suspensions were sonicated for 20 min shortly before use to prevent aggregate formation.

Characterization of nTiO$_2$ was conducted as follows: The shapes of nTiO$_2$ in suspension were imaged by transmission electron microscopy (TEM) and scanning electron microscopy (SEM). Element analysis was performed by a an X-ray microanalyzer (EDAX, Tokyo, Japan), after aliquots of nTiO$_2$ were loaded onto a carbon sheet. For size distribution analysis, aliquots of the 500 μg/ml nTiO$_2$ suspension were loaded onto clean glass slides and photographed under a polarized light microscope (Olympus BX51N-31P-O polarized light microscope, Tokyo, Japan), and the photos were then analyzed by an image analyzer system (IPAP, Sumika Technos Corporation, Osaka, Japan). Over 1000 particles of anTiO$_2$ and rnTiO$_2$ were measured.

Animals

Female Sprague-Dawley rats (SD rats) were purchased from CLEA Japan Co., Ltd (Tokyo, Japan). The animals were housed in the animal center of Nagoya City University Medical School, maintained on a 12 hour light-dark cycle and received oriental MF basal diet (Oriental Yeast Co., Tokyo, Japan) and water *ad lib*. The research was conducted according to the Guidelines for the Care and Use of Laboratory Animals of Nagoya City University Medical School and the experimental protocol was approved by the Institutional Animal Care and Use Committee (H22M-19).

Trans-tracheal intra-pulmonary spraying (TIPS) protocol

Three groups of 6 female SD rats (Group 1, saline; Group 2, anTiO$_2$; and Group 3, rnTiO$_2$) aged 9 weeks were acclimated for 7 days prior to the start of the study. Saline and nTiO$_2$ suspensions were administered by TIPS to the animals under isoflurane anesthesia: The nozzle of a Microsprayer (series IA-1B Intratracheal Aerosolizer, Penn-century, Philadelphia, PA) connected to a 1 ml syringe was inserted into the trachea through the larynx and a total volume of 0.5 ml suspension was sprayed into the lungs synchronizing with spontaneous inspiration by the animal (Xu et al., 2010). Rats were treated once every the other day over a 2 week period, a total of eight treatments. The total amount of anTiO$_2$and rnTiO$_2$ administered to Groups 2 and 3 was 2.0 mg per rat. Six hours after the last spraying, the animals were killed and the whole lung was excised and divided into two parts; the left lung was cut into pieces and immediately frozen at -80°C and used for biochemical analysis, and the right lung was fixed in 4% paraformaldehyde solution in phosphate-buffered saline (PBS) adjusted to pH 7.3 and processed for immunohistochemical, light microscopic and transmission electron microscopic (TEM) examinations.

Light microscopy and transmission electron microscopy

Hematoxylin and eosin (H&E) stained sections were used for pathological observation. The number of alveolar macrophages in H&E lung tissue slides was counted and expressed as number per mm^2.

Slides were observed under light microscopic observation, the corresponding area in the paraffin block was cut out, deparaffinized and embedded in epoxy resin and processed for TEM and titanium element analysis with a JEM-1010 transmission electron microscope (JEOL Co. Ltd, Tokyo, Japan) equipped with an X-ray microanalyzer (EDAX, Tokyo, Japan).

Analysis of 8-hydroxydeoxy guanosine levels

For the analysis of 8-hydroxydeoxyguanosine (8-OHdG) levels, genomic DNA was isolated from a piece of the left lung with a DNA Extractor WB kit (Wako Chemicals Co. Ltd). 8-OHdG levels were determined with an 8-OHdG ELISA Check kit (Japan Institute for Control of Aging, Shizuoka, Japan).

RNA isolation, cDNA synthesis and RT-PCR analysis of gene expression

Pieces of the left lungs (50-100 mg) were thawed, rinsed 3 times with ice cold PBS, and total RNA was isolated using 1 ml Trizol Reagent (Invitrogen, Karlsruhe, Germany). For reverse transcription PCR (RT-PCR) and real-time PCR, first strand cDNA synthesis from 2 mg of total RNA was performed using SuperScript™ III First-Strand Synthesis

System (Invitrogen of Life Technologies, CA) according to the manufacturer's instructions. PCR primers for rat MIP1α were 5'-TTTTGAGACCAGCAGCCTTT -3' (forward) and 5'- CTCAAGCCCCTGCTCTACAC-3' (reverse), and the product size was 191bp. b-actin was used as internal control and the primers were 5'- AGCCATGTACGTAGCCATCC-3' (forward) and 5'-CTCTCAGCTGTGGTGGTGAA-3', and the product size was 228 bp. RT-PCR was conducted using an iCycler (BioRad Life Sciences, CA) as follows: 95°C 20 sec, 60°C 20 sec, 72°C 30sec, 30 cycles for MIP1α; and 95°C 20 sec, 60°C 20 sec, 72°C 30sec, 15 cycles for b-actin. Real-time PCR analysis of MIP1α gene expression was performed with a 7300 Real Time PCR System (Applied Biosystem, CA) using Power SYBR Green PCR Master Mix (Applied Biosystem, CA) according to the manufacturer's instructions. b-actin gene was used as the normalizing reference gene.

Immunohistochemical analysis

Paraffin embedded lung tissues sections were immunostained with polyclonal anti-rat MIP1α (BioVision, Lyon, France). Antigen retrieval was carried out by microwave for 20 min in 10 mmol/L citrate buffer (pH 6.0). Antibody was diluted 1:100 in blocking solution and applied to the slides, and the slides were incubated at 4°C overnight. Immunohistochemical staining was done by the avidin-biotin complex method (ABC) using the Vectastain Elite ABC system (Vector Laboratories, Burlingame, CA). Biotinylated goat anti-rabbit IgG (Vector Laboratories) was used as a secondary antibody at a dilution of 1:500 for 1 hour and visualized using avidin-conjugated alkaline phosphatase complex (ABC kit, Vector laboratories) and Alkaline Phosphatase Substrate Kit (Vector Laboratories). Sections were lightly counterstained with hematoxylin for microscopic examination.

ELISA for MIP1α in the lung tissues and the supernatants of cell culture

Left lung tissue samples (50-100mg) were thawed, rinsed 3 times with ice cold PBS and homogenized in 1 ml of tissue extraction reagent (PeproTech, London, UK) containing 1% (v/v) Proteinase Inhibitor Cocktail (Sigma-Aldrich, St Louis, MO, USA). The homogenates were clarified by centrifugation at 10,000g, 4°C for 5 min. The protein content in the supernatants was measured with a BCATM Protein assay kit (Pierce). The levels of MIP1α in the supernatants were measured using rat MIP1α ELISA Development Kit (Cat#: 900-K75, Peprotech, Inc., Rocky Hill, NJ.) according to the manufacturer's instruction, and expressed as pg/mg lung tissue protein. The levels of MIP1α in cell culture supernatants were measured as described above and expressed as pg/ml.

Isolation of PAM and exposure of $nTiO_2$ to PAM cells

Induction and isolation of alveolar macrophages in female SD rats was performed as described previously (Xu et al., 2010). 10^6 primary alveolar macrophages (PAM) were cultured in RPMI1640 containing 2% fetal bovine serum and antibiotics overnight at 37°C, 5% CO_2. 500 μg/ml of $anTiO_2$ and $rnTiO_2$ suspensions was then added to the cultures to a final concentration of 10 μg/ml and the cells were incubated for another 24 hours. RNA was isolated from the PAM and the level of MIP1α protein in the conditioned culture media was measured by ELISA.

In vitro cell proliferation assay

A549 cells were seeded into 96-well culture plates at 2×10^3 cells per well in 2% fetal bovine serum Dulbecco's modified Eagle's medium (Wako Chemicals Co., Ltd). After overnight incubation, the medium was replaced with the conditioned PAM culture media treated with $anTiO_2$ or $rnTiO_2$, and the cells were incubated for another 72 hours, with or without 20 μg/ml of anti-MIP1α neutralizing antibody (R&D Systems, Minneapolis, MN). The relative cell number of A549 cells was determined using a Cell counting Kit-8 (Dojindo Molecular Technologies, Rockville, MD) according to the manufacturer's instruction.

Cytotoxicity assay in vitro

A549 cells, the primary human lung fibroblast cell line CCD34 (ECACC, Cat. No. 90110514) and PAM were used for cytotoxicity analyses. Cells were seeded in 96 well plates at 5×10^3/well and incubated overnight. The cells were then treated with $anTiO_2$ and $rnTiO_2$ suspensions at final concentrations of 0, 2, 10, or 50 μg/ml and then incubated for another 24 hours. The relative cell number was determined as described above.

Cytotoxicity of $anTiO_2$ and $rnTiO_2$ under ultraviolet B irradiation

A549 cells were used for analysis of $nTiO_2$ cytotoxicity under ultraviolet irradiation. First, we determined an irradiation time that did not affect the cell viability as follows: A549 cells were seeded into 96 well plates at 1×10^3/well in 200 μL Dulbecco's modified Eagle's medium (Wako Chemicals Co., Ltd) containing 10% fetal bovine serum and incubated overnight. The cells were irradiated with ultraviolet B (UVB) for 0, 30 sec, 1 min, 2 min, 5 min and 10 min with a transilluminator (Vilber Lourmat, France). The light intensity was 1000 mW/cm^2, and the emission spectrum was from 270 nm to 330 nm with a peak at 312 nm. The non-irradiated control wells were covered with a sterile aluminium sheet to prevent irradiation. The relative cell number was determined after incubation for 48 hours at 37°C, 5% CO_2.

Next, we observed the effect of $anTiO_2$ and $rnTiO_2$ on cell viability under UVB. A549 cells were seeded into 96 well plate at 1×10^3well in 100 μL culture media and incubated overnight. Then, 100 mL of $anTiO_2$ or $rnTiO_2$ suspensions in DMEM culture medium containing 10% FBS was added into the wells to final concentration of 0, 2, 5 and 10 μg/ml and incubated for 30 min. The cells were irradiated with UVB for 2 min (2 min UVB irradiation did not affect cell viability), and incubated for another 48 hours, before determination of relative cell number.

Statistical and analysis

Statistical significance of the *in vitro* and *in vivo* findings was analyzed using the two-tailed Student's t-test. *In vitro* and *in vivo* data are presented as means±standard

deviations. A value of $p<0.05$ was considered to be significant.

Results

Characterization of $nTiO_2$ particles in suspension

TEM images showed that individual $anTiO_2$ particles were spherical in shape, while individual $rnTiO_2$ particles had a rod-like shape, and both $anTiO_2$ and $rnTiO_2$ formed large aggregates in suspension (Figure. 1A and B). Similarly, SEM observation indicated aggregate formation of both types of $nTiO_2$ particles (Figure. 1C and D). Peaks of titanium (green arrows) and oxygen (blue arrows), which are present in both types of $nTiO_2$ particles, and carbon (white arrows) and nitrogen (red arrow), which are present in the carbon sheets used in the SEM, were observed by elemental scanning (Figure. 1E and F). Peaks of other elements were not detected in either the $rnTiO_2$ or $anTiO_2$ samples. Analyses of particle size showed that the mean and medium diameters were 5.491±2.727 mm and 5.127 mm for $anTiO_2$, and 3.799±2.231 mm and 3.491 mm for $rnTiO_2$ (Figure. 1G), confirming aggregate formation of both types of $nTiO_2$ particles in suspension.

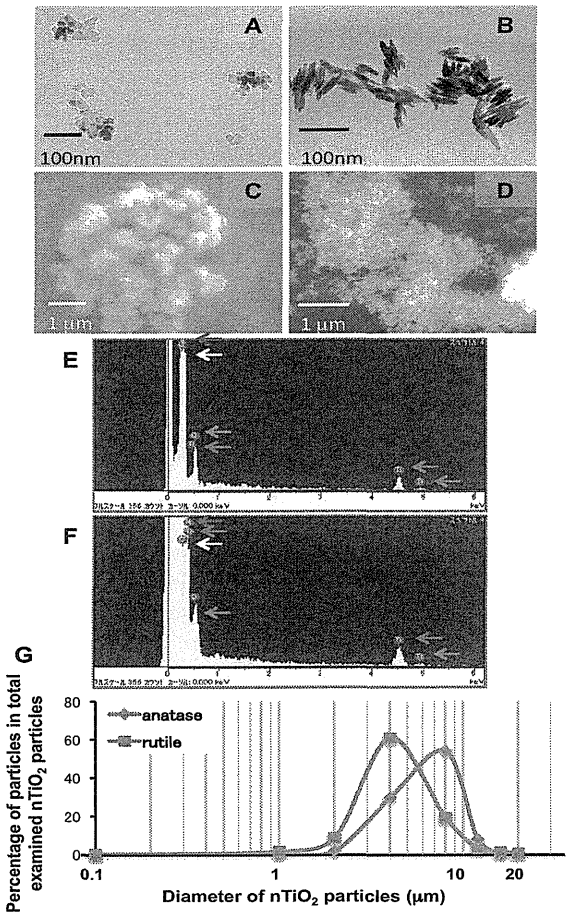

Figure 1. Characterization of $nTiO_2$ Particles in Suspension. A and B: TEM imagines of $anTiO_2$ and $rnTiO_2$ particles in suspension. C and D: SEM images of $anTiO_2$ and $rnTiO_2$ particles. E and F: Element scanning showed peaks of titanium (green arrows), oxygen (blue arrows), carbon (white arrows) and nitrogen (red arrows) in $anTiO_2$ and $rnTiO_2$ particles. G: Size distribution of $anTiO_2$ and $rnTiO_2$ in suspension

Histological observation and 8-OHdG level in the lung tissue

Only a few small lung inflammatory lesions were observed in rats treated with $anTiO_2$ and $rnTiO_2$ (Figure. 2A, B and C). Alveolar macrophage infiltration was found throughout the lung tissue, and most of the alveolar macrophages were seen with phagocytosed $anTiO_2$ particles or $rnTiO_2$ particles (Figure. 2D, E an F). TEM observation demonstrated that both $anTiO_2$ and $rnTiO_2$ were deposited in various sizes in the cytoplasm of the alveolar macrophages (Figure. 2G and H). Neither $anTiO_2$ or $rnTiO_2$ particles were found in other types of cells in the lung tissue. The number of macrophages per mm^2 lung tissue section was 67.1±15.8 (saline), 165.0±34.9 ($anTiO_2$) and 214.2±44.1 ($rnTiO_2$). The numbers of macrophages in the $anTiO_2$ and $rnTiO_2$ treated groups was significantly higher than in the control group ($p<0.001$), and the $anTiO_2$ treated group had lower macrophage infiltration than the $rnTiO_2$ treated group.

The level of 8-OHdG, a parameter of oxidative DNA damage caused by reactive oxygen species (ROS), in the lung tissue in rats treated with $anTiO_2$ and $rnTiO_2$ was 1.96±0.77 and 3.07±1.25 (pg per mg DNA), respectively, and was higher than that of the control (1.44±0.63): The increase in 8-OHdG in the lungs of $rnTiO_2$, but not $anTiO_2$, treated rats was significantly higher than the control

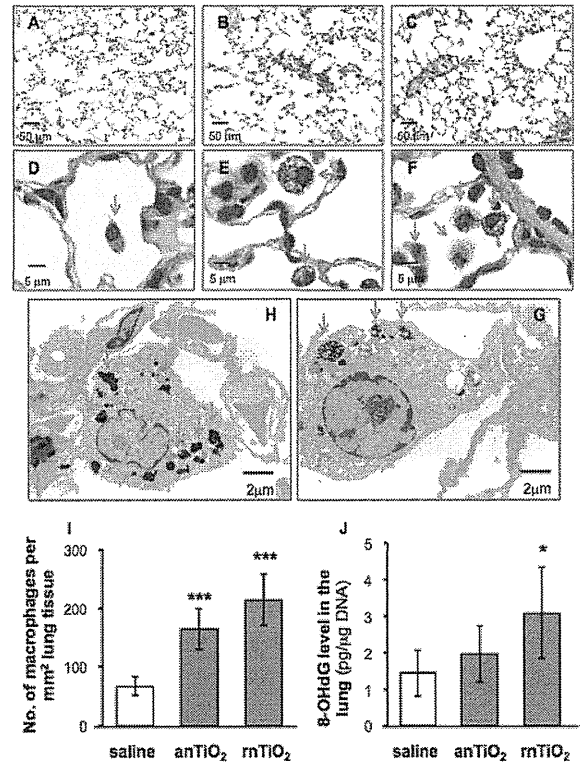

Figure 2. Histological Observation and 8-OHdG Level in the Lung Tissue. A, B and C: Histological imagines of lung tissue treated with saline, $anTiO_2$ and $rnTiO_2$, respectively. Green arrows indicate small inflammatory lesions. D (saline), E ($anTiO_2$) and F ($rnTiO_2$): Higher magnification imagines of alveolar macrophages (brown arrows). $nTiO_2$ particles are clearly observed. G and H: TEM imagines of alveolar macrophages with $anTiO_2$ and $rnTiO_2$ particles in their cytoplasm (blue arrows). I and J: The numbers of alveolar macrophages and 8-OHdG levels in the lung tissue. *, *** represent $p<0.05$ and 0.001, respectively, versus saline

($p<0.05$) (Figure. 2J).

MIP1α expression in the lung tissue

RT-PCR suggested an increase in MIP1α mRNA expression in lung tissue treated with $anTiO_2$ or $rnTiO_2$ (Figure. 3A). Real-time PCR analysis indicated that compared with the control group, the increase was 2.79-fold for $anTiO_2$ and 5.35-fold for $rnTiO_2$. MIP1α mRNA expression was also significantly lower in the $anTiO_2$ treated group compared to the $rnTiO_2$ treated group (Figure. 3B). The levels of MIP1α protein in the lung tissue were 32.8±0.31 and 52.7±0.58 pg/mg lung protein in the $anTiO_2$ and $rnTiO_2$ treated groups, both significantly higher than that of the control group (20.8±0.24) (Figure. 3C). Similarly to MIP1α mRNA expression, MIP1α protein expression was significantly lower in the $anTiO_2$ treated group compared to the $rnTiO_2$ treated group.

To find out what cells in the lung accounted for the increased MIP1α protein expression, we examined tissue samples using MIP1α immunohistochemistry. As shown in Figure. 3D, E and F, MIP1α protein was produced by $anTiO_2$ or $anTiO_2$ burdened alveolar macrophages.

Exposure of PAMs to $anTiO_2$ and $rnTiO_2$ and cell proliferation assays in vitro

As in the lung tissue, *in vitro* exposure of PAM to $nTiO_2$ induced expression of MIP1α mRNA (Figure. 4A) and protein (Figure. 4B). Treatment with $anTiO_2$ and $rnTiO_2$ caused 11.96-fold and 15.26-fold increases in the expression of MIP1α mRNA, respectively, in cultured PAM. The level of MIP1α protein in the cell culture medium was 32.8±1.1 pg/mL for $anTiO_2$ and 52.7±1.3 pg/mL for $rnTiO_2$, significantly higher than that of the control

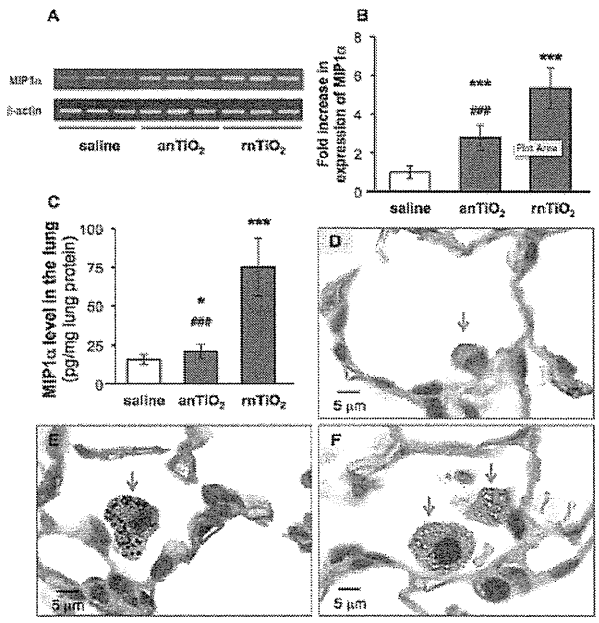

Figure 3. Expression of MIP1α in the Lung Tissue. A, B and C: Analysis of expression of MIP1α mRNA by RT-PCR (A) and real-time PCR (B) and protein by ELISA (C). D, E, and F: Immunohistochemistry shows MIP1α expressed in alveolar macrophages of lung tissue treated with saline (D), $anTiO_2$ (E) and $rnTiO_2$ (F). *, *** represent $p<0.05$ and 0.001, respectively, versus saline; ### represent $p<0.001$, versus $rnTiO_2$

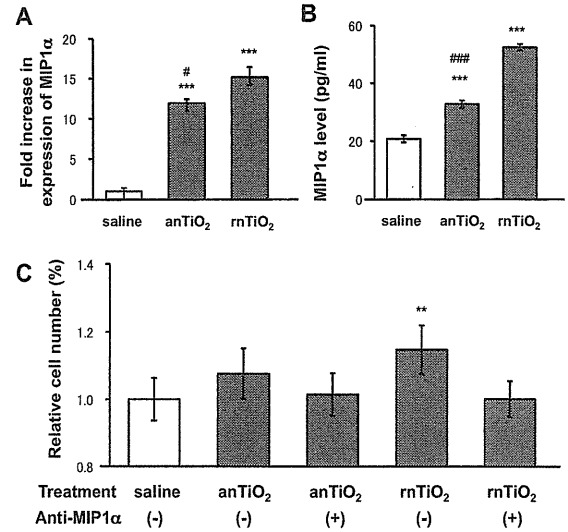

Figure 4. The Effect of $anTiO_2$ and $rnTiO_2$ on PAM Cells. The expression of MIP1α mRNA in cultured PAM (A) and protein in the culture media (B) indicate that treatment with $anTiO_2$ or $rnTiO_2$ increased MIP1α expression in the PAM. Conditioned cell culture media of PAM treated with $rnTiO_2$, but not $anTiO_2$, had a significant effect on proliferation of A549 cells, and this promotion was attenuated by addition of 20 μg/ml MIP1α neutralizing antibody (C). **, ***represent $p<0.01$ and 0.001, versus saline; #, ###represent $p<0.05$ and 0.001, versus $rnTiO_2$

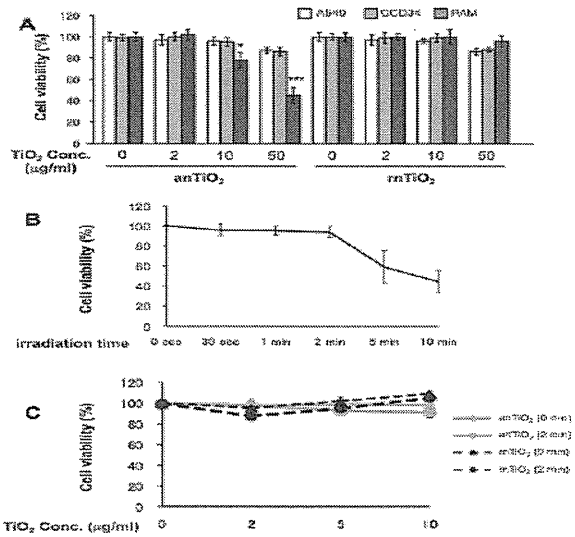

Figure 5. *In vitro* Assays. A: The effect of $anTiO_2$ and $rnTiO_2$ on the viability of A549, CCD34 and PAM cells. B: The effect of UVB irradiation on the viability of A549 cells. C: The effect of $anTiO_2$ and $rnTiO_2$ on the vi ability of A549 under UVB irradiation. *, *** represent $p<0.05$ and 0.001, versus the vehicle

(20.8±1.2 pg/mL). Both mRNA and protein expression of MIP1α was significantly lower in the $anTiO_2$ treated PAM compared to the $rnTiO_2$ treated cells.

The supernatants of the culture media of PAM treated with $anTiO_2$ showed only a tendency to increase A549 cell proliferation, while those collected from PAM treated with $rnTiO_2$ significantly promoted proliferation of A549 cells (115%) compared to supernatants from the saline treated group (Figure. 4C). The promotion effect of the supernatants of PAM cell cultures treated with $anTiO_2$or

rnTiO$_2$ was attenuated by anti-MIP1α neutralizing antibodies, indicating MIP1α is probably a mediator of the increase in A549 cell proliferation.

In vitro cytotoxicity assays

In vitro cytotoxicity assays indicated that both anTiO$_2$ and rnTiO$_2$ had little effect on the cell viability of A549 and CCD34 cells at a concentration of up to 50 mg/ml. anTiO$_2$ had a cytotoxic effect on the cell viability of PAM at doses of 10 and 50 mg/ml, while rnTiO$_2$ did not impair the cell viability of PAM at any of the examined concentrations (Figure. 5A).

To investigate whether UVB irradiation affected the cytotoxic effects of anTiO$_2$ and rnTiO$_2$ on cell viability, we first determined the exposure times that ultraviolet B irradiation itself did not impair the viability of A549 cells. As shown in Figure. 5B, irradiation for up to 2 min did not have any effect on the viability of A549 cells. With 2 min of UVB irradiation, neither anTiO$_2$ or rnTiO$_2$ at doses of 2, 5 or 10 μg/ml resulted in any decrease in the viability of A549 cells (Figure. 5C).

Discussion

The toxicity of nanoparticles usually includes tiers of biological responses such as induction of ROS and inflammation (Nel et al., 2006). This may contribute to carcinogenic potential (Tsuda et al., 2009). Thus, in the present study, we compared several parameters ofr inflammation and oxidative stress induced by TIPS of anTiO$_2$ and rnTiO$_2$. The results indicated that both anTiO$_2$ and rnTiO$_2$ particles were phagocytosed by alveolar macrophages and did not cause strong lung inflammation. Treatment with anTiO$_2$ and rnTiO$_2$ increased alveolar macrophage infiltration, MIP1α expression and 8-OHdG production: anTiO$_2$ had less effect than rnTiO$_2$.

Phagocytosis by alveolar macrophages is a major defense mechanism for deposition and clearance of inhaled particles (Heppleston, 1984; Rom et al., 1991; Geiser et al., 2008). However, activation of alveolar macrophages is strongly associated with inflammatory reactions and ROS production (Renwick et al., 2001; Bhatt et al., 2002; Wang et al., 2007). Also, MIP1α, secreted from rnTiO$_2$ burden alveolar macrophages, is possibly involved in the promotion of lung carcinogenesis (Xu et al., 2010). Similarly, pleural macrophage recruitment and activation are involved in the pathogenesis of asbestos (Choe et al., 1997). These results indicate two contrasting roles of alveolar macrophages in pathogenesis and host defense.

The toxic effects of nanoparticles are dependent on their size, shape, surface functionality and composition (Albanese et al., 2012). In the present study, we used comparable sizes of anTiO$_2$ and rnTiO$_2$ particles. Both types of nTiO$_2$ had no surface coating and had no obvious difference in elemental composition. Therefore, differences in alveolar macrophage induction, MIP1α expression and 8-OHdG production between anTiO$_2$ and rnTiO$_2$ are likely due to their different crystal structures and shapes. The lower toxicity of anTiO$_2$ compared to rnTiO$_2$ in the absence of UVB irradiation in our study is consistent with a previous *in vitro* study with bulk rutile and anatase TiO$_2$ (Gurr et al., 2005). In contrast to a previous study (Sayes et al., 2006), in the present study anTiO$_2$ and rnTiO$_2$ did not exhibit different toxicities on the cell viability of A549 cells under ultraviolet irradiation.

It should be noted that both types of anTiO$_2$ and rnTiO$_2$ particles formed aggregates in suspension, and aggregation may alter their bio-reactivity. Whether anTiO$_2$ and rnTiO$_2$ particles have different long-term effects remains to be clarified.

In conclusion, *in vivo* exposure of the rat lung to anTiO$_2$ or rnTiO$_2$ particles increased alveolar macrophage infiltration, MIP1α expression and 8-OHdG production, with anTiO$_2$ eliciting lower levels of biological responses than rnTiO$_2$. Similarly, exposure of primary alveolar macrophages to rnTiO$_2$ *in vitro* resulted the cells producing more MIP1α mRNA and protein than cells exposed to anTiO$_2$. Cytotoxicity assays *in vitro* indicated that both anTiO$_2$ and rnTiO$_2$ had very low cellular toxicity even under UVB irradiation.

Acknowledgements

This work was supported by Health and Labour Sciences Research Grants (Research on Risk of Chemical substance, H19-kagaku-ippan-006 and H22-kagaku-ippan-005). We thank Chisato Ukai and Takako Narita for their excellent secretarial assistance for the work.

References

Albanese A, Tang PS, Chan WC (2012). The effect of nanoparticle size, shape, and surface chemistry on biological systems. *Annu Rev Biomed Eng*, **14**, 1-16.

Bhatt NY, Kelley TW, Khramtsov VV, et al (2002). Macrophage-colony-stimulating factor-induced activation of extracellular-regulated kinase involves phosphatidylinositol 3-kinase and reactive oxygen species in human monocytes. *J Immunol*, **169**, 6427-34.

Choe N, Tanaka S, Xia W, et al (1997). Pleural macrophage recruitment and activation in asbestos-induced pleural injury. *Environ Health Perspect*, *105*, 1257-60.

Geiser M, Casaulta M, Kupferschmid B, et al (2008). The role of macrophages in the clearance of inhaled ultrafine titanium dioxide particles. *Am J Respir Cell Mol Biol*, **38**, 371-6.

Gurr JR, Wang AS, Chen CH, et al (2005). Ultrafine titanium dioxide particles in the absence of photoactivation can induce oxidative damage to human bronchial epithelial cells. *Toxicology*, **213**, 66-73.

Heppleston AG (1984). Pulmonary toxicology of silica, coal and asbestos. *Environ Health Perspect*, **55**, 111-27.

IARC (2010). Carbon black, titanium dioxide, and talc. *IARC Monogr Eval Carcinog Risks Hum*, **93**, 1-413.

Kakinoki K, Yamane K, Teraoka R, et al (2004). Effect of relative humidity on the photocatalytic activity of titanium dioxide and photostability of famotidine. *J Pharm Sci*, **93**, 582-9.

Maynard AD, Aitken RJ, Butz T, et al (2006). Safe handling of nanotechnology. *Nature*, **444**, 267-9.

Mohr U, Ernst H, Roller M, et al (2006). Pulmonary tumor types induced in Wistar rats of the so-called "19-dust study". *Exp Toxicol Pathol*, **58**, 13-20.

Nel A, Xia T, Madler L, et al (2006). Toxic potential of materials at the nanolevel. *Science*, **311**, 622-7.

Renwick LC, Donaldson K, Clouter A (2001). Impairment of alveolar macrophage phagocytosis by ultrafine particles.

Toxicol Appl Pharmacol, **172**, 119-27.

Rom WN, Travis WD, Brody AR (1991). Cellular and molecular basis of the asbestos-related diseases. *Am Rev Respir Dis*, **143**, 408-22.

Sayes CM, Wahi R, Kurian PA, et al (2006). Correlating nanoscale titania structure with toxicity: a cytotoxicity and inflammatory response study with human dermal fibroblasts and human lung epithelial cells. *Toxicol Sci*, **92**, 174-85.

Schulte P, Geraci C, Zumwalde R, et al (2008). Occupational risk management of engineered nanoparticles. *J Occup Environ Hyg*, **5**, 239-49.

Tsuda H, Xu J, Sakai Y, Futakuchi M, Fukamachi K (2009). Toxicology of engineered nanomaterials - A review of carcinogenic potential. *Asian Pac J Cancer Prev*, **10**, 975-980.

Wang H, Li J, Quan X, et al (2007). Formation of hydrogen peroxide and degradation of phenol in synergistic system of pulsed corona discharge combined with TiO_2 photocatalysis. *J Hazard Mater*, **141**, 336-43.

Wu J, Liu W, Xue C, et al (2009). Toxicity and penetration of TiO_2 nanoparticles in hairless mice and porcine skin after subchronic dermal exposure. *Toxicol Lett*, **191**, 1-8.

Xu J, Futakuchi M, Iigo M, et al (2010). Involvement of macrophage inflammatory protein 1alpha (MIP1alpha) in promotion of rat lung and mammary carcinogenic activity of nanoscale titanium dioxide particles administered by intra-pulmonary spraying. *Carcinogenesis*, **31**, 927-35.

Arch Toxicol
DOI 10.1007/s00204-013-1086-5

INORGANIC COMPOUNDS

Nanosized zinc oxide particles do not promote DHPN-induced lung carcinogenesis but cause reversible epithelial hyperplasia of terminal bronchioles

Jiegou Xu · Mitsuru Futakuchi · David B. Alexander · Katsumi Fukamachi · Takamasa Numano · Masumi Suzui · Hideo Shimizu · Toyonori Omori · Jun Kanno · Akihiko Hirose · Hiroyuki Tsuda

Received: 25 February 2013 / Accepted: 20 June 2013

Abstract Zinc oxide (ZnO) is known to induce lung toxicity, including terminal bronchiolar epithelial hyperplasia, which gives rise to concerns that nanosized ZnO (nZnO) might lead to lung carcinogenesis. We studied the tumor promoting activity of nZnO by an initiation–promotion protocol using human c-Ha-*ras* proto-oncogene transgenic rats (H*ras*128 rats). The rats were given 0.2 % N-nitrosobis(2-hydroxypropyl)amine (DHPN) in the drinking water for 2 weeks and then treated with 0.5 ml of 250 or 500 μg/ml nZnO suspension by intra-pulmonary spraying once every 2 weeks for a total of 7 times. Treatment with nZnO particles did not promote DHPN-induced lung carcinogenesis. However, nZnO dose-dependently caused epithelial hyperplasia of terminal bronchioles (EHTB) and fibrosis-associated interstitial pneumonitis (FAIP) that were independent of DHPN treatment. Tracing the fate of EHTB lesions in wild-type rats indicated that the hyperplastic lesions almost completely disappeared within 12 weeks after the last nZnO treatment. Since nZnO particles were not found in the lung and $ZnCl_2$ solution induced similar lung lesions and gene expression profiles, the observed lesions were most likely caused by dissolved Zn^{2+}. In summary, nZnO did not promote carcinogenesis in the lung and induced EHTB and FAIP lesions that regressed rapidly, probably due to clearance of surplus Zn^{2+} from the lung.

Keywords Nanosized zinc oxide particles · Lung toxicity · Lung carcinogenesis · Epithelial hyperplasia of terminal bronchioles · Interstitial pneumonitis · Lung fibrosis

Electronic supplementary material The online version of this article (doi:10.1007/s00204-013-1086-5) contains supplementary material, which is available to authorized users.

J. Xu · D. B. Alexander · H. Tsuda (✉)
Laboratory of Nanotoxicology Project, Nagoya City University, 3-1 Tanabedohri Mizuho-ku, Nagoya 467-8603, Japan
e-mail: htsuda@phar.nagoya-cu.ac.jp

J. Xu · M. Futakuchi · K. Fukamachi · T. Numano · M. Suzui
Department of Molecular Toxicology, Nagoya City University Graduate School of Medical Sciences, 1-Kawasumi, Mizuho-cho, Mizuho-ku, Nagoya 467-8601, Japan

H. Shimizu
Core Laboratory, Nagoya City University Graduate School of Medical Sciences, 1-Kawasumi, Mizuho-cho, Mizuho-ku, Nagoya 467-8601, Japan

T. Omori
Department of Health Care Policy and Management, Nagoya City University Graduate School of Medical Sciences, 1-Kawasumi, Mizuho-cho, Mizuho-ku, Nagoya 467-8601, Japan

J. Kanno · A. Hirose
National Institute of Health Sciences, 1-18-1 Kamiyoga, Setagaya-ku, Tokyo 158-8501, Japan

Introduction

One of the most widely used nanomaterials is nZnO. The worldwide production of nZnO powder is increasing every year and was reported to have reached 1.4 million tons in 2011. It is used in rubber industry and electronics and in commercial products such as sunscreens and paints. In the biomedical field, it is used in baby powders, antiseptic ointments, and zinc oxide tapes to treat a variety of skin conditions (Baldwin et al. 2001; Hughes and McLean 1988). Recently, nZnO has gained interest in cancer applications or as an active anticancer drug (Rasmussen et al. 2010).

Micron or larger-sized ZnO particles are considered to be "Generally Recognized as Safe" (GRAS) in food

Published online: 06 July 2013

additives by the FDA. However, exposure to fumes containing ZnO and other metal particles during welding or galvanizing processes is known to lead to metal fume fever (Antonini et al. 2003; Drinker and Fairhall 1933; Fine et al. 1997). Recent reports have shown that nZnO affects cell viability and induces reactive oxygen species (ROS) in many mammary cell types in tissue culture (Deng et al. 2009; Lee et al. 2008; Xia et al. 2008; Yang et al. 2009), cause proliferation of airway epithelial cells, goblet cell hyperplasia, interstitial pulmonary inflammation and fibrosis (Cho et al. 2011), and reversible inflammatory reaction in the bronchoalveolar lavage fluid in animal studies (Sayes et al. 2007; Warheit et al. 2009). nZnO also leads to DNA damage (Kermanizadeh et al. 2012) and micronuclei formation in vitro (Valdiglesias et al. 2013). While these in vitro and in vivo studies have provided some information on acute toxic effects of nZnO on certain cell types and animals, further in vivo studies are needed to determine whether nZnO has chronic toxic effects as in some other metal oxide particles. For example, epidemiological data indicate that exposures of aluminum oxide or iron oxide lead to pneumoconiosis in human (Hull and Abraham 2002; Sano 1963); titanium dioxide has carcinogenic activity in the rat lung (Heinrich et al. 1995; Xu et al. 2010). Such chronic toxicity data will have more impact on risk assessment of nZnO.

Since nZnO induces inflammatory reaction, ROS production, and genotoxicity, which are implicated in cancer development, in the present study, we tested the lung carcinogenicity of nZnO by an initiation–promotion protocol using human c-Ha-*ras* proto-oncogene transgenic (H*ras* 128) rats, which have the same susceptibility to chemically induced lung carcinogenesis as their parent wild-type rats, but are highly susceptible to mammary tumor induction (Tsuda et al. 2005). The results indicated that nZnO did not have promotion effect on DHPN-induced lung and mammary carcinogenesis and caused reversible EHTB and FAIP.

Materials and methods

Animals

Forty-three female transgenic rats carrying the human c-Ha-RAS proto-oncogene (H*ras*128 rats) and 42 female wild-type Sprague–Dawley rats were obtained from CLEA Japan Co., Ltd. (Tokyo, Japan). The animals were housed in the Animal Center of Nagoya City University Medical School and maintained on a 12-h light/12-h dark cycle and received Oriental MF basal diet (Oriental Yeast Co. Ltd., Tokyo, Japan) and water ad libitum. The study was conducted according to the Guidelines for the Care and Use of Laboratory Animals of Nagoya City University Medical School, and the experimental protocol was approved by the Institutional Animal Care and Use Committee (H22M-19).

Preparation, characterization of nZnO suspensions, and administration of nZnO to the lung

Zinc oxide particles (CAS No. 1314-13-2, MZ-500, without coating, with a mean primary diameter of 25 nm) were obtained from Tayca Cooperation, Osaka, Japan. The particles were suspended in 0.1 % Tween 20 saline at 250 or 500 μg/ml. The suspension was sonicated for 20 min to prevent aggregate formation.

Characterization of nZnO was conducted as follows: the shape of nZnO in the suspensions was imaged by transmission electron microscopy (TEM); element analysis was performed by an X-ray microanalyzer (EDAX, Tokyo, Japan), after aliquots of nZnO were loaded on a carbon sheet; the size distribution of nZnO in the 500 μg/ml suspension was analyzed using a Particle Size Distribution Analyzer (Shimadzu Techno-Research, Inc., Kyoto, Japan). The characterization results are shown in Figure S1.

Before being administrated to rats, the nZnO suspensions were further sonicated for 20 min. 0.5 ml of the nZnO suspensions was administrated to the lung by intra-pulmonary spraying (IPS) as described previously (Xu et al. 2010).

Carcinogenicity study

The carcinogenic activity of nZnO was assessed in female H*ras*128 rats using an initiation–promotion protocol by which we used previously to evaluate lung and mammary carcinogenicity of titanium dioxide nanoparticles (Xu et al. 2010). Briefly, three groups of 10–11 female H*ras*128 rats aged 6 weeks were given 0.2 % DHPN (Wako Chemicals, Co., Ltd. Osaka, Japan) in the drinking water for 2 weeks, and Groups 4 and 5 (6 rats each) were given drinking water without DHPN. Two weeks later, Group 1 and Group 4 were administered 0.1 % Tween 20 saline, and Group 2, Group 3, and Group 5 were administered 250, 500, and 500 μg/ml nZnO suspensions by IPS once every two weeks from the end of week 4 to week 16, a total of 7 times. The total amounts of nZnO administered to Groups 1, 2, 3, 4, and 5 were 0, 0.875, 1.75, 0, and 1.75 mg/rat, respectively. The dosing was determined according to the permissible exposure limit for zinc oxide particles of the Occupational Safety and Health Administration (OSHA) (see Discussion). Three days after the last treatment, animals were killed and the organs (brain, lung, liver, spleen, kidney, mammary gland, ovaries, uterus, and neck lymph nodes) were fixed in 4 % paraformaldehyde in PBS buffer adjusted to pH 7.3 and processed for histological examination and transmission electron microscopy (TEM).

Light microscopy, polarized light microscopy, and transmission electron microscopy

Hematoxylin–Eosin (H&E)-stained pathological slides of the lung and other major organs were used to observe nZnO with a light microscope and polarized light microscope (PLM) (Olympus BX51N-31P-O polarized light microscope, Tokyo, Japan) at 1,000× magnification. Localization of the illuminated particles was confirmed in the same H&E-stained sections after removing the polarizing filter.

Paraffin blocks were deparaffinized and embedded in epon resin and processed for nZnO observation and zinc element analysis, using a JEM-1010 transmission electron microscope (TEM) (JEOL, Co. Ltd, Tokyo, Japan) equipped with an X-ray microanalyzer (EDAX, Tokyo, Japan).

Immunohistochemistry and Azan–Mallory staining

PCNA was detected using an anti-PCNA monoclonal antibody (Clone PC10, Dako Japan Inc., Tokyo, Japan). The antibody was diluted 1:200 in blocking solution and applied to deparaffinized slides, and the slides were incubated at 4 °C overnight. The slides were then incubated for 1 h with biotinylated species-specific secondary antibodies diluted 1:500 (Vector Laboratories, Burlingame, CA) and visualized using avidin-conjugated horseradish peroxidase complex (ABC kit, Vector Laboratories). To assess lung fibrosis, paraffin-embedded slides were deparaffinized, and collagen fibers were visualized by Azan–Mallory staining.

Reversibility study and effects of $ZnCl_2$ solution

To assess whether nZnO-induced terminal bronchiolar epithelial hyperplasia, interstitial pneumonitis, and lung fibrosis are reversible, we conducted reversibility experiments. Seven groups of 5 female wild-type Sprague–Dawley rats aged 10 weeks were administrated 0.5 ml of 0.1 % Tween 20 saline or 500 μg/ml nZnO suspension by IPS 2 times per week for 4 weeks. Group 1 was treated with 0.1 % Tween 20 saline and killed 1 day after the last IPS. Groups 2–7 were treated with 0.5 ml of 500 μg/ml nZnO suspension and killed at 1 day and 2, 4, 6, 8, and 12 weeks after the last IPS. For the comparison of the effects of zinc ion and nZnO, Group 8 was treated with 0.5 ml of 6.17 mM $ZnCl_2$ solution (the molecular amount is equal to that of 500 μg/ml nZnO suspension) by IPS at the same frequency and time period as the nZnO groups and killed 1 day after the last IPS. The left lung was cut into pieces and frozen in liquid nitrogen for biochemical analysis, and the right lung was processed for histological examination. Other major organs were excised for histological examination, and the blood was collected for cytological and biochemical analysis.

Gene expression analysis

The left lungs from Groups 1, 2, and 8 in the reversibility study described above were used for isolation of RNA. RNA was isolated by using TRizol reagent (Invitrogen of Life Technologies, CA).

For microarray analysis, 1 μg RNA from each rat of Group 1 was combined and 1 μg RNA from each rat of Group 2 was combined. The quality of the 2 mixtures of RNA samples was assessed and quantified using the Agilent 2100 BioAnalyzer RNA Nano chip system (Agilent Technologies, CA) prior to further manipulation. Microarray analysis was conducted by the 3-D Gene Chip (Toray Industries Inc., Kanagawa, Japan), and a total of 20,000 genes were analyzed. Microarray-based pathway analysis was performed by Toray Industries Inc., Kanagawa, Japan.

For reverse transcription-PCR (RT-PCR) and real-time PCR, first-strand cDNA synthesis from 1 μg of RNA was performed using SuperScript™ III First-Strand Synthesis System (Invitrogen of Life Technologies, CA) according to the manufacturer's instructions. Primers are as follows: forward primer, 5′-TAGAATCGAGGTGCACAGGAGT-3′, reverse primer, 5′-TATTCCAGCAGGCTGTCAAAGA-3′, product size, 228 bp for Orm1; forward primer, 5′-AAGTGGAGGAGCAGCTGGAGTGG-3′, reverse primer, 5′-CCAAAGTAGACCTGCCCGGACTC-3′, product size, 155 bp for Tnfa, and forward primer, 5′-AGCCATGTACGTAGCCATCC-3′, reverse primer, 5′-CTCTCAGCTGTGGTGGTGAA-3′, product size, 228 bp for Actb. RT-PCR was conducted using an iCycler (BioRad Life Sciences, CA) as follows: 95 °C 20 s, 60 °C 20 s, 72 °C 30 s, 30 cycles for Orm1; 95 °C 20 s, 60 °C 20 s, 72 °C 20 s, 25 cycles for Tnfa, and 95 °C 20 s, 60 °C 20 s, 72 °C 30 s, 15 cycles for Actb. Real-time PCR analysis of Orm1 and Tnfa gene expression was performed with the 7300 real-time PCR system (Applied Biosystem, CA) using the premix reagent Power SYBR Green PCR Master Mix (Applied Biosystem, CA) according to the manufacturer's instructions. The Actb gene was used as the normalizing reference gene.

Determination of zinc ion

For detection of Zn^{2+} content in the lung tissue, 50–100 mg of the frozen lung tissues from the reversibility study described above were thawed at room temperature, rinsed with cold PBS 3 times, and homogenized for 30 s at the highest speed in 1 ml of T-PER, tissue protein extraction reagent (Pierce, Rockford, IL), with Polytron R PT 2100 homogenizer (Capitol Scientific Inc., TX). The homogenates were clarified by centrifugation at 10,000×g for 15 min at 4 °C, and the supernatants were used for Zn^{2+}

detection. Zn^{2+} detection was performed using QuantiChrom™ Zinc Assay kit (BioAssay Systems, CA) according to the manufacturer's instructions.

In vitro nZnO dissolution assay

5 μl of 500 μg/ml nZnO suspension (2.5 μg/tube) and increasing amounts of 1 mg/ml human α 1 acid glycoprotein (Sigma-Aldrich, product number G9885) or bovine serum albumin (Sigma-Aldrich, product number A2058) were added to microtubes, and the total volume of each tube was adjusted to 100 μl with 0.1 % Tween 20 saline. The final protein concentration of human α 1 acid glycoprotein or bovine serum albumin was 0, 100, 200, 300, 400, and 500 μg/ml. The tubes were then incubated at 37 °C for 2 h. The nZnO particles were removed by centrifugation at 10,000×*g* for 5 min, and Zn^{2+} concentration in the supernatants was determined as described above.

In vitro cytotoxicity assay

The induction and preparation of rat primary alveolar macrophages (PAM) has been described (Xu et al. 2010). 5×10^3 PAMs, 1×10^3 A549 cells (human lung adenocarcinoma cell line), and 2×10^3 CCD34 cells (human lung fibroblast cell line) were seeded into 96-well culture plates and cultured overnight in 100 ml of RPMI 1,640 containing 10 % FBS. The cells were added with nZnO suspension or ZnCl2 solution to final concentrations of 0, 1, 5, or 25 μg/ml of nZnO and 0, 12.3, 61.7, or 308.6 nM of ZnCl2 (1, 5, and 25 μg/ml of nZnO are equal to 12.3, 61.7, and 308.6 nM of ZnCl2, respectively, in the amount of zinc element) and incubated for another 72 h. The cell viability was then determined using the Cell Counting Kit-8 (Dojindo Molecular Technologies, Rockville, MD) according to the manufacturer's instruction.

Statistical analysis

Statistical analysis was performed using ANOVA. Statistical significance was analyzed using a two-tailed Student's *t*-test. A p value of <0.05 was considered to be significant.

Results

Carcinogenesis study in H*ras*128 rats

DHPN-induced lung alveolar cell hyperplasia and adenoma development was used for the end point observation to assess the carcinogenicity of nZnO in our medium-term assay. As shown in Table 1, the incidence and multiplicity (number/cm^2 lung tissue section) of

Table 1 Effect of nZnO on lung proliferative lesions in H128-*ras* rats

Treatment	No. of rats	DHPN-induced proliferative lesions						DHPN-independent EHTB[a]	
		ACH[a]		Ade[a]		ACH + Ade		Inc. (%)	Multiplicity[b] (no./cm^2 lung)
		Inc.[a] (%)	Multiplicity[b] (no./cm^2 lung)	Inc. (%)	Multiplicity[b] (no./cm^2 lung)	Inc. (%)	Multiplicity[b] (no./cm^2 lung)		
DHPN + vehicle	11	11 (100)	2.43 ± 1.29	2 (18.1)	0.09 ± 0.20	11 (100)	2.52 ± 1.26	0 (0)	0
DHPN + 250 μg/ml nZnO	10	10 (100)	1.64 ± 1.09	3 (30.0)	0.12 ± 0.19	10 (100)	1.76 ± 1.03	7 (70)	0.86 ± 0.86 **
DHPN + 500 μg/ml nZnO	10	10 (100)	1.83 ± 1.05	5 (50.0)	0.30 ± 0.31	10 (100)	2.13 ± 1.23	10 (100)	4.93 ± 1.95 ***
Vehicle	6	0	0	0	0	0	0	0	0
500 μg/ml nZnO	6	2 (33.3)	0.16 ± 0.26	0	0	2 (33.3)	0.16 ± 0.26	6 (100)	3.91 ± 1.29 ***

[a] ACH, Ade, EHTB, and Inc. are abbreviations for alveolar cell hyperplasia, adenoma, epithelial hyperplasia of terminal bronchioles, and incidence, respectively

[b] Multiplicity is expressed as mean ± s.d

** and *** represent p values <0.01 and 0.001, respectively, versus DHPN + vehicle or vehicle

alveolar cell hyperplasia and adenoma in the groups treated with nZnO were not significantly different from the DHPN alone group. In the rats which received nZnO treatment without prior DHPN treatment, alveolar cell proliferation foci, recognized as thickening of the alveolar wall with proliferative alveolar epithelium, were observed, but significant differences from the saline group were not observed. In the mammary gland, significant inter-group difference in incidence and multiplicity of mammary tumors was also not observed (data not shown).

A notable lesion induced in all the nZnO-treated groups was epithelial hyperplasia of terminal bronchioles (EHTB). The EHTB lesions had increased cell density, often with the epithelial cells arranged in 1–3 layers, and partly extended bronchiolar structures with transition to the normal

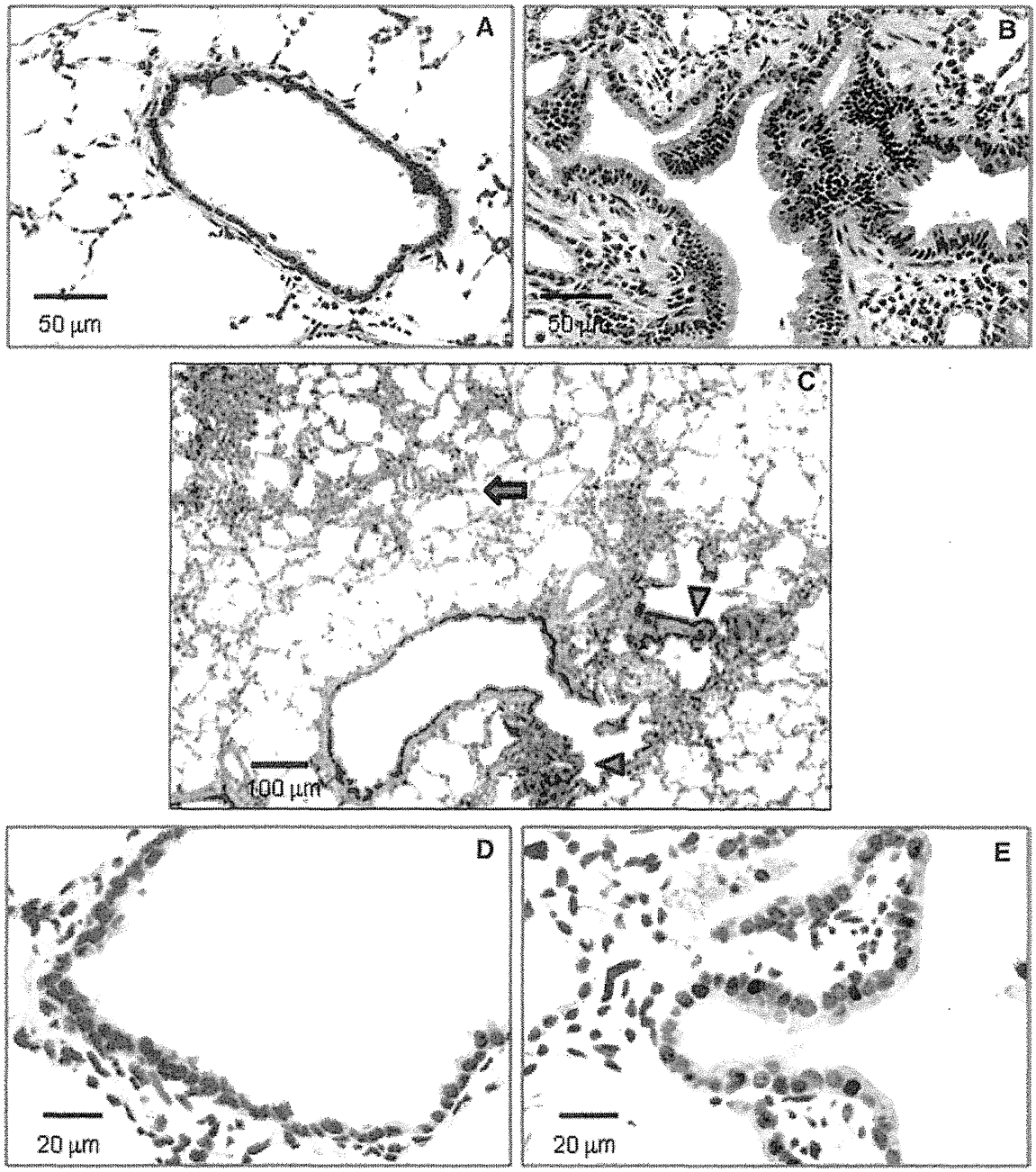

Fig. 1 Induction of EHTB by nZnO. **a** representative normal terminal bronchiolar epithelium (NTBE); **b** EHTB in H&E-stained slides; **c** images and localizations of DHPN-induced alveolar hyperplasia (*arrow*) and nZnO-induced EHTB (*arrow heads*); **d** images of PCNA immunostaining in NTBE; and **e** in EHTB